

TWO PHOTON OPTOGENETIC STIMULATION OF CELLS

by

KAMAL RAJ DHAKAL

Presented to the Faculty of the Graduate School of
The University of Texas at Arlington in Partial Fulfillment
of the Requirements
for the Degree of

MASTER OF SCIENCE IN PHYSICS

THE UNIVERSITY OF TEXAS AT ARLINGTON

December 2012

Copyright © by Kamal Dhakal 2012

All Rights Reserved



Acknowledgements

Foremost, I would like to express my sincere gratitude to my advisor, Prof. Samarendra Mohanty, of his continuous support of Master's study and research. I am immensely inspired by his motivation, enthusiasm, and immense knowledge in optics and biochemistry. His guidance helped me in research and writing this thesis.

I would also like to express sincere gratitude to members of my master's thesis evaluation committee (Prof. Ali R. Koymen, Prof. Mario Romero and Graduate Advisor Prof. Ashok Ray) for reviewing this thesis document and offering insightful comments and advice.

I acknowledge my fellow research group members, S. Shivalingaiah, Ling Gu, Ting Li, T.S Dennis and Rahul Patil who worked together on various parts of these projects. I am equally grateful to and Prof. Linda Perrotti and Bryan Black for their contributions.

Last but not the least; I would like to thank my parents; Chandrakala Dhakal and Laxmi Prasad Dhakal for giving birth to me in the first place and instilling in me spirituality and moral values throughout my life. I am equally thankful to my wife Bishnu Devi Regmi and son Ishan Dhakal.

November 21, 2012

Abstract

TWO-PHOTON OPTOGENETIC STIMULATION OF CELLS

Kamal Dhakal

The University of Texas at Arlington, 2012

Supervising Professor: Samarendra Mohanty

The controlled stimulation of cells, especially neurons, is of significant interest both for basic understanding of neuronal circuitry as well as clinical interventions. Existing electrode-based methods of stimulation are invasive and non-specific to highly localized regions or specific cell types. Recently, optical stimulation of targeted neurons expressing light-sensitive proteins (opsins) using visible light has emerged as a powerful technique in neuroscience. However, the use of these optogenetic tools as a minimally invasive technique for in-vivo applications is limited to the study/intervention of superficial regions of the brain since, due to absorption and scattering, a significant amount of the visible light is lost as depth of penetration increases. Therefore, the deep-brain (at depths > 1 mm) optogenetic stimulation of neurons in behaving animals is equally invasive as the electrical stimulation since it requires delivery of light in close proximity to the cells of interest. It has been recently shown that by non-linear interaction of light with opsin, *in-vitro* two-photon stimulation using near-infrared (NIR) light is possible. While these experiments used microscope objectives to stimulate cells *in vitro*, this thesis reports *in vivo*, in-depth fiber-optic two-photon optogenetic stimulation (FO-TPOS) of neurons in mouse models. In order to optimize the deep-brain stimulation strategy, two-photon activation efficacy at different near-infrared laser parameters (average power density, wavelength, exposure, etc.) were characterized. The significantly-enhanced depth

stimulation efficiency of FO-TPOS as compared to conventional single-photon beam was demonstrated both by experiments and Monte Carlo simulation. Manipulation of depth neuronal circuitry in ventral tegmental area (VTA) of the midbrain was achieved using FO-TPOS and confirmed by immunohistochemistry. FO-TPOS as demonstrated in this report will lead to a better understanding of *in- vivo* neural circuitry, and may help in therapeutic modulation of brain activity because this technology permits precise (few micron) and less invasive anatomical delivery of stimulation with high spatial and temporal specificity.

Table of Contents

Acknowledgements	iii
Abstract	iv
Table of Contents	vi
List of Illustrations	viii
Chapter 1 Introduction.....	1
1.1 Optogenetics.....	1
1.2 Application of optogenetics.....	5
1.3 Advantages of two-photon.....	5
Chapter 2 Theory and Experimental Setup.....	8
2.1 Two-photon fluorescence excitation	8
2.2 Patch-clamping and recording.....	8
2.3 <i>In-vivo</i> recording	11
2.4 Light Propagation Model.....	12
2.5 Monte-Carlo Modeling	14
2.6 Stimulation theory	16
2.7 Channelrhodopsin-2 dynamics	20
Chapter 3 Materials and Methods.....	22
3.1 Cell culture	22
3.2 Optogenetic stimulation	22
3.3 Patch-clamp recording.....	23
3.4 Monte Carlo simulation.....	24
3.5 Mouse preparation.....	25
3.6 <i>In vivo</i> optrode recordings	25
3.7 <i>In vivo</i> electrophysiology recordings.....	26

3.8 Statistics	26
Chapter 4 Results and Discussion	27
4.1 <i>In vitro</i> FO-TPOS irradiation leads to optogenetic stimulation	27
4.2 Peak FO-TPOS stimulation wavelength is also blue shifted	32
4.3 <i>In vivo</i> FO-TPOS stimulation is intensity dependent.	35
4.4 Comparison of depth penetration between two-photon and single- photon stimulation.....	41
4.5 FO-TPOS is direct stimulation	49
Chapter 5 Conclusions and Future Work.....	54
5.1 Conclusions	54
5.2 Future work.....	55
Appendix A Parameters of Monte-Carlo Simulation	58
References.....	60
Biographical Information	70

List of Illustrations

Figure 1.1 Schematic diagram showing method of probing functional relationship.	1
Figure 1.2 Optogenetics: Steps involving in optogenetics.	4
Figure 1.3 Comparison of two-photon and single photon fluorescence excitation.	6
Figure 1.4 Schematic comparison: (a) single-photon blue excitation	7
Figure 2.1 Jablonski diagram of (a) single –photon (b) two-photon excitation.	8
Figure 2.2 Patch clamp set up for FO-TPOS.	10
Figure 2.3 <i>In-vivo</i> optogenetic stimulation using single (blue) vs two-photon	12
Figure 2.4 Geometry of light from fiber.	13
Figure 2.5 Geometry used for Monte-Carlo Simulation.	14
Figure 2.6 A flow chart showing simplified model of Monte-Carlo Simulation.	16
Figure 2.7 Schematic diagram (a) two-photon fluorescence	19
Figure 3.1 Laboratory set up for (a) in-vitro recording	23
Figure 3.2 Laboratory set up for in-vivo recording.	26
Figure 4.1 <i>In-vitro</i> two-photon activation of ChR2-expressing cells	28
Figure 4.2 Current response due to control laser beam	30
Figure 4.3 Peak amplitude of current with function of power density	31
Figure 4.4 (a) Schematic of two-photon stimulation of targeted neuron	33
Figure 4.5 (a) Peak voltage vs. wavelength of <i>in-vivo</i> FO-TPOS	35
Figure 4.6 Direct two-photon illumination of micropipette-electrode.	37
Figure 4.7 (a) <i>In-vivo</i> raw spiking of locally stimulated neurons	39
Figure 4.8 (a) Variation of peak amplitude of single photon	41
Figure 4.9 Monte Carlo simulation of light propagation	42
Figure 4.10 Monte Carlo (MC) simulation of light propagation in two-layered cortex.	44
Figure 4.11 (a) Raw spiking activity at different depths	46

Figure 4.12 (a) Variation of peak amplitude of FO-TPOS.....	47
Figure 4.13 Variation of peak amplitude of two-photon activated electrical recording.	48
Figure 4.14 Histogram of peak-amplitude as a function of power densities	49
Figure 4.15 Sketch showing depth stimulation limit of fiber-optic	51
Figure 4.16 (a) Overlay of raw spikes (red profiles) with shutter	52
Figure 4.17 (a) histogram of latency of spikes.....	53
Figure 5.1 Comparison of microscopic two-photon setup.....	55

Chapter 1

Introduction

1.1 Optogenetics

Francis Crick, in his article "Unrealized prerequisites for assembling a general theory of the mind," observed that the ability to manipulate individual units of the brain would be required "a method by which all neurons of just one type could be inactivated, leaving the others more or less unaltered" [1]. While high resolution neuronal imaging has enabled the mapping of the physical connectome [2] of the brain in a high-throughput manner, there is now a growing need for an efficient, high resolution method to functionally map the multitude of neural connections in the brain.

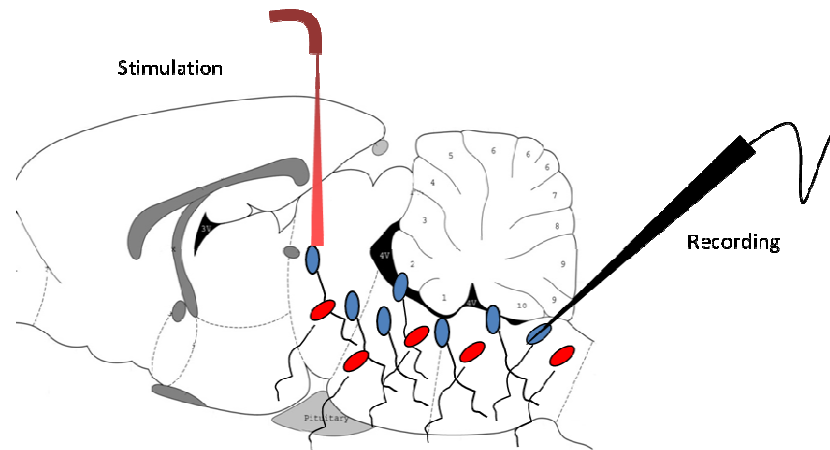


Figure 1.1 Schematic diagram showing method of probing functional relationship between neurons at different location: red and blue are different types of neuron.

There are various techniques which directly or indirectly map the structure of the brain, such as MRI and fluorescent (transparent) brain imaging [3]. However, understanding the functional relationships among neurons located in different regions of

brain (Figure 1.1) is challenging by electrical stimulation methods, as these methods lack the required specificity. Attempts have been made to manipulate extracellular electrical activities (i.e. electric stimulation) within specified volume. This may have allowed the temporal precision, but lacks the specificity. Pharmacological and genetic manipulations can target specific cells with certain expression profiles, but they lack temporal precision on the timescale of neural coding and signaling (i.e. milliseconds) [4]. In fact, until recently, no existing method could achieve both the temporal precision and spatial resolution required for selective neuronal activation within neural network of billions of cells. Optogenetics, on the other hand, is able to excite or inhibit in millisecond temporal scale and with cellular specificity. Recently, visible light-assisted activation of selected neuronal groups have been made possible with high temporal precision by introducing a light-activated molecular channel; channelrhodopsin-2 (ChR2) [5-7] or its variants. As shown in Figure 1.2, genes coding for Channelrhodopsin-2, derived from algae, is transfected and expressed in desired cells to be studied. Upon irradiation, cells expressing ChR2 are stimulated. This method has several advantages over electrical stimulation [8-10], such as cellular specificity and minimal invasiveness. Therefore optogenetics is growing as a valuable tool in neuroscience research. However, as the use of light-activated molecular ChR2 for *in-vivo* models is increasing, neuroscientists are rapidly discovering the limitations of its utility. Although optogenetic methods require very low intensity light ($1-10 \text{ mW/mm}^2$) [6], at the activation wavelength for ChR2 (460 nm), significant absorption and scattering of stimulating light occurs, which leads to limited (shallow) penetration of the beam [11]. Thus, in order to stimulate cells in the ventral tegmentum area of the brain, one has to choose between one of two undesirable alternatives: The first is to maintain the minimally invasive qualities of the approach but requires that the average blue light beam power be significantly increased.

Unfortunately, this approach often leads to significant deleterious effects on the cells' viability in the vicinity of the target, and thus severely limits the translational potential of this technology. The second alternative approach is to use optical fiber [12-14] or μ LED[15]-based blue light delivery to excite neurons which are in close proximity to the optical fiber or μ LED. This approach severely compromises the minimally invasive quality of optogenetics because optical fibers (similar to electrodes used in electrical stimulation techniques) or μ LED(s) need to penetrate through more superficial brain tissue in order to reach ventral (3-4 mm deep) brain regions. In this way, the superficial brain tissue gets damaged; and such damage can lead to difficulty in interpreting the outcome of deep-brain stimulation. Therefore, several attempts have been made to shift the activation peak of ChR2 from the blue to the red wavelength region [16-18], where biological tissue absorption and scattering is reduced. While there has been some success at the cost of altered light-activation kinetics, it seems near-infrared opsins would be ideal for in-depth cell-specific optogenetic stimulation of excitable cells in an organism. However, the success in developing a near-infrared opsin would still not permit applicability of the method for selective activation of specific regions in deep (ventral) brain areas, since the single-photon (red or infrared) stimulating beam will also stimulate neurons outside of the targeted population as shown in Figure 1.4b.

The technique of using light to activate microbial opsin in biological interventions is a long tradition. Chromophore-assisted laser can inhibit the targeted protein by inactivation. So laser has been used to inhibit targeted proteins by destroying them what a geneticist would call "loss of function" [19]. Again, lasers can be used to stimulate neurons or cells directly (such as genetically targeted opsin-expressing cells) what a geneticist would call "gain of function" [20]. These microbial opsins are widely found

everywhere in the world which after interactions with the light, acts as open channel for non-specific ions.

The read out for activation of neurons (by light or other means) is primarily obtained through electrical means though optical read out methods are emerging [21-24]. Understanding of mechanism of brain or whole nervous system became more clear when Hodgkin and Huxley developed a theoretical model of the electrical signal, so called action potential, via which neurons communicate [25]. This model assumes axon as charged capacitor and ion channels as resistor forming an electrical circuit. Whenever there is conductance of ions across the ion channels, electrical signals are produced [26], commonly known as action potential. Understanding of mechanism of brain is widely-expanded by implementation of physics and electronics together [27]. The use of optogenetics, that combines genetics and optics to modulate and control the activity of specific neurons or cells, is now widely adopted in neuroscience.

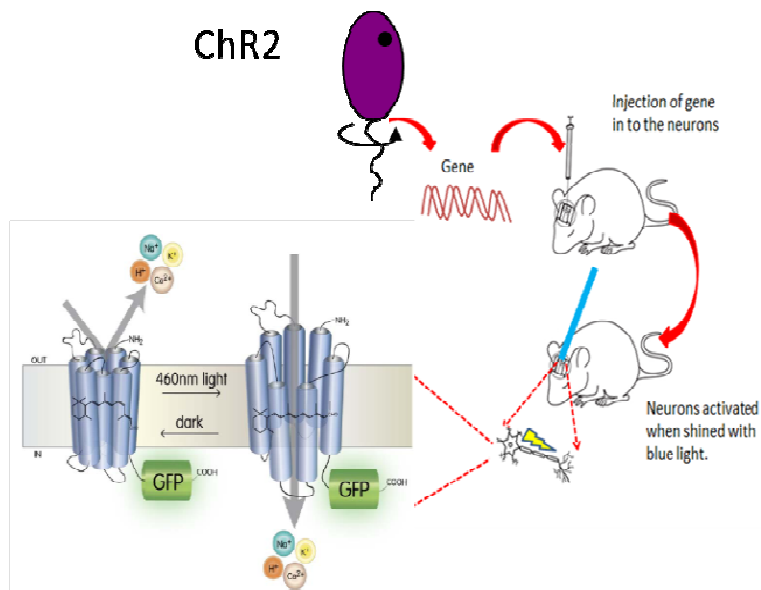


Figure 1.2 Optogenetics: Steps involving in optogenetics.

<http://www.sciencedirect.com/science/article/pii/S0896627306002248>

1.2 Application of optogenetics

Application of optogenetics has been rapidly increasing with many researchers are being attracted towards this field while use of opsins and its mutants is allowing sensitization of specific neuronal networks *in vitro* as well as *in vivo*. Advancement in technology such as development of spatially-modulated laser beams, millisecond shutter, scanning devices and focusing optics is necessary for realizing full-potential of this technology. In recent years, researchers in this field have shown interesting experiments controlling the activity of behaving animal by inserting one end of fiber in head of freely behaving mice and other end coupled to the laser beam. Those experiments were able to modulate learning [28], wakening [29] , somatosensation [30], vision [31], breathing [32] and movement [33]. In 2009, it was demonstrated that ChR2 can be used safely to stimulate neuron without effecting the immune system and death of neurons in non-human brain [34].

1.3 Advantages of two-photon

Deep brain stimulation is one widely used method to treat patients suffering from muscle tremors, stiffness, impaired or slowed movement, and partial paralysis, such as those with Parkinson's disease [35]. Treatment provided through deep brain stimulation can block abnormal nerve signals [36] and to reduce or eliminate neurological movement disorders. Conversely, deep brain stimulation can be employed to facilitate the firing of many neurons simultaneously, which can lead to the release of hormones like oxytocin [37]. However, electrode-based stimulation is neither temporally nor spatially precise. Furthermore, electrode-based methods can lead to contamination of tissues in the vicinity of the electrodes. If we can stimulate deep brain tissues optically, it would be much more advantageous than electrical stimulation in several ways. Optogenetics with single photon excitation may replace the conventional stimulation methods. However, due to

high absorption and scattering coefficients, visible light, which is the widely used spectrum in optogenetics cannot reach in inner depth of the brain. The two-photon optogenetic activation using a near infrared laser beam can provide both deep penetration and high spatial precision, achieved by virtue of the non-linear nature of ultrafast light interaction as shown in Figure 1.3 and Figure 1.4c.

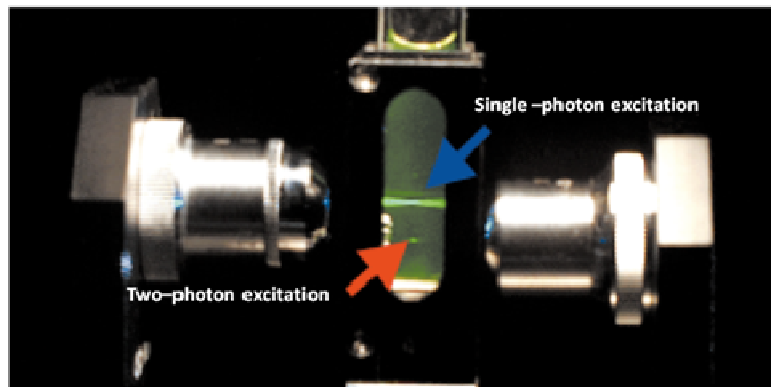


Figure 1.3 Comparison of two-photon and single photon fluorescence excitation.

Source: <http://www.c-km.org.tw/message/92/92.htm>

Since the first demonstration[38] of *in-vitro* two-photon optogenetic stimulation (TPOS) of ChR2-sensitized cells by using point or scanning laser beam, there has been significant progress [39-41] in using TPOS for probing neural circuitry in cultured neuronal cells as well as brain slices. Furthermore, recent advances demonstrate that optogenetically-sensitized neurons can be activated by spatially-sculpting [40] and/or temporal-focusing the TPOS beam [41]. It is important to note that the two-photon cross-section of ChR2 is estimated to be ~300 times (Lucifer yellow $0.95 \pm 0.2 \text{ GM}$) [42] than that of most of the fluorophores at same wavelength and therefore has potential for stimulating opsin-expressing neurons using weakly-focused (and even defocused) two-photon beams. However, two-photon excitation has only been demonstrated *in vitro* with microscope-based set-up [38, 39, 43]. In this study, *in-vivo* fiber-optic two-photon

optogenetic stimulation (FO-TPOS) of in-depth neuronal circuitry in transgenic mouse model is demonstrated.

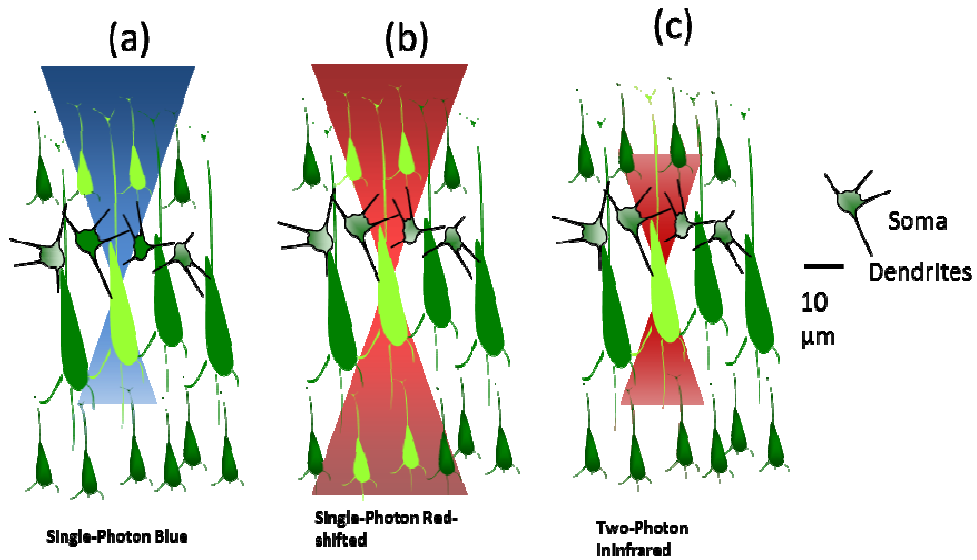


Figure 1.4 Schematic comparison: (a) single-photon blue excitation, (b) single-photon red-shifted excitation and (c) two-photon optogenetic stimulation (TPOS)

Chapter 2

Theory and Experimental Setup

2.1 Two-photon fluorescence excitation

Two-photon excitation is based on the idea that two-photons of approximately half of energy that needed for single photon excitation can also excite atoms or molecules in one quantum event. Each photon carries approximately [44] half the energy necessary to excite the molecule. These two-photons should hit the excitable molecule virtually at the same time with high density of photon. Since the two-photon cross-section is extremely low, this process requires high density of photons, available from ultrafast laser sources. The two-photon excitation or transition of molecule is proportional to the square of the intensity, a non-linear process [45] .

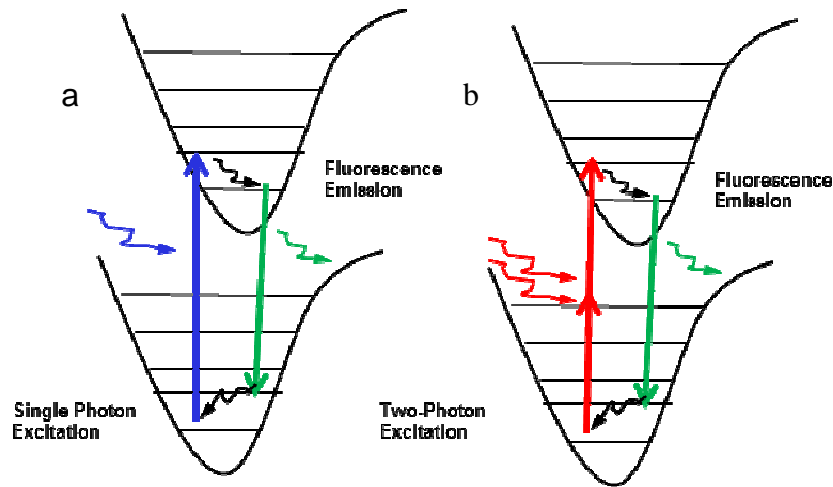


Figure 2.1 Jablonski diagram of (a) single –photon: molecule gets excited to higher state by absorbing a photon gives light fluorescence during relaxation and (b) two-photon excitation.

2.2 Patch-clamping and recording

The opto-electrophysiology setup was developed on the Olympus-Upright laser-microscope platform (Figure 2.2), using a computer-controlled amplifier system (Axon

Multiclamp 700B, Molecular Devices Inc., USA). Parameters of the pipette puller were optimized to obtain the desired borosilicate micropipettes of resistance from 3 to 7 M Ω for a whole-cell patch clamp. Two stage The micropipette was filled with a intra-cellular solution containing (in mM) 130 K-Gluconate, 7 KCl, 2 NaCl, 1 MgCl₂, 0.4 EGTA, 10 HEPES, 2 ATP-Mg and 0.3 GTP-Tris (pH 7.4). The electrode head stage was mounted on a XYZ micromanipulator (Newport Inc.). The standard extracellular solution containing (in mM): 150 NaCl, 10 Glucose, 5 KCl, 2 CaCl₂, 1 MgCl₂ was buffered with 10mM HEPES (pH 7.3). The output from the amplifier was digitized using a National Instruments DAQ card (PCI 6221). For electrophysiological recording, the hardware was interfaced with patch-clamp software from the University of Strathclyde (Glasgow, UK; noncommercial use). Electrical recordings were performed at a holding potential of -60mV at room temperature (20 - 24°C). The whole system was built on a vibration isolation table (Newport Inc.) and electrical isolation was done by means of a Faraday cage that was placed around the setup. Aluminum foil was used wherever necessary to reduce noise level. Temperature of cells and its environment is crucial in the experiment. Temperature of the stage was adjusted during the patch-clamp by monitoring the thermometer.

The Ti:Sapphire laser wavelength was tuned from 800 nm to 920 nm using computer-controlled software, to compare the wavelength-dependent efficacy in stimulating the targeted ChR2-sensitized and control cells. The number of pulses at each point of irradiation was controlled by a computer-controlled mechanical shutter (S). The power of the fs (femto second) laser beam was varied by controlling the orientation of a circular variable neutral density filter (NDF). The laser beam power at the focal plane was measured using a power meter (PM100D, Thorlabs Inc.). Using motorized stage movement, the region of interest was aligned with the center of the focused/defocused spot. The precise positioning of the spot on the cell was carried out by controlling the

galvo-scanning mirrors (SM) using data acquisition and control system based on LabView (National Instruments Inc.). For activation of ChR2-expressing cells (identified by YFP fluorescence), the optogenetic stimulation beam (473 nm, or NIR) was delivered via a 50 μm core optical fiber, mounted on a mechanical micromanipulator so as to position the tip of the fiber near the desired cell being patch-clamped. For generating and controlling pulses of light, the electromechanical shutter in the laser beam path was interfaced with a PC. TTL pulses of desired frequency were generated using National Instruments (PCI 6221) card in order to generate required laser pulses for activation. For electrophysiological measurements subsequent to optical activation, the shutter was synchronized with the patch clamp recording electrode. The whole system was built on a vibration isolation table (Newport Inc.) pClamp software was used to analyze the data.

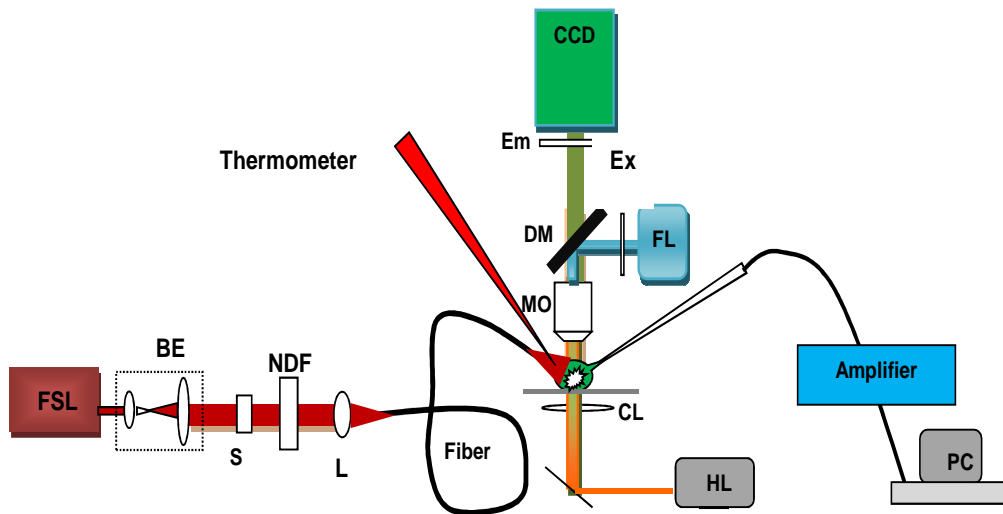


Figure 2.2 Patch clamp set up for FO-TPOS. FSL: Tunable Ti: Sapphire Laser; BE: Beam Expander; S: Shutter; NDF: Neutral density filter; L: Lens for fiber coupling; FL: Fluorescence excitation source; Ex: Excitation Filter; Em: Emission Filter; MO: Microscope Objective; CL: Condenser lens; DM: Dichroic Mirror; M: Mirror; HL: Halogen Lamp.

2.3 In-vivo recording

To determine the variation of in-vivo two-photon activation efficacy as a function of average laser power density (intensity), the ChR2-expressing cortical regions of the transgenic mice were stimulated using the setup shown in Figure 2.3(a). Furthermore, to compare the intensity-dependency of in-vivo two-photon stimulation with that of single-photon, a blue diode laser (473 nm) was combined with the two-photon laser beam using a dichroic mirror (DM), co-aligned by a folding mirror (M), expanded by beam expander (BE) and coupled to a single fiber using a lens (FL). A computer-controlled shutter (S) was used (Figure 2.3a) to control the stimulation pulse duration and the frequency of both the single and two-photon activation beams. In order to rule out photoactivation of the recording electrodes, which would lead to spurious signals, the optical fiber was affixed (shown by white line in right inset in (Figure 2.3c) to a glass micro-pipette with the fiber-tip positioned ~1 mm of the pipette tip. A tungsten electrode was inserted into the pipette containing extracellular recording solution ~2 cm away from the fiber tip. Loss of some near-infrared light from the fiber can be seen near the shank of the pipette tip due to bending of the fiber. Figure 2.3b shows two-photon optogenetic stimulation of anesthetized mice placed in stereotaxic set up.

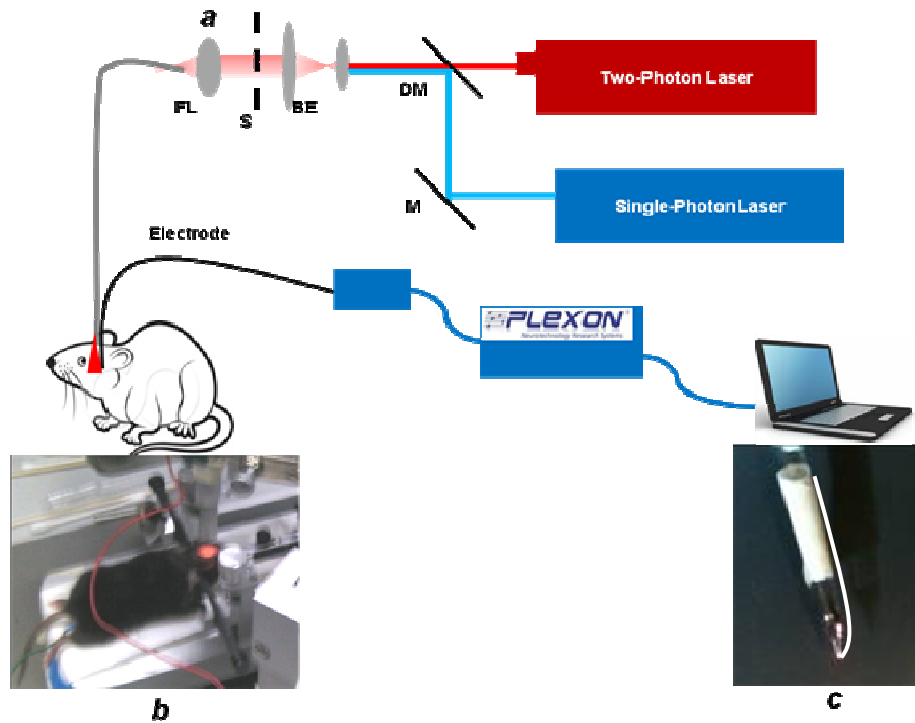


Figure 2.3 *In-vivo* optogenetic stimulation using single (blue) vs two-photon (NIR) stimulation. (a) Set-up for *in-vivo* single and two-photon optogenetic stimulation and electrophysiological recording, (b) FO-TPOS stimulation of anesthetized mice, (c) Glass electrode and fiber (shown by white line) based optrode.

2.4 Light Propagation Model

All of our experiments were conducted with the optical fiber kept perpendicular to the area of stimulation, unless otherwise noted. While considering optics there are mainly four factors attributed to the distribution of light emitting from the fiber. These are

- Light source.
- Geometry of spreading.
- Scattering of light by tissue.
- Absorption of light by tissue.

The light irradiance (I) in space at each point given by the source light irradiance at the center of fiber (I_0) can be defined by the following equation.

$$I(r,z) = G(r,z) C(z) \Phi(z) I_0 \quad (2.4.1)$$



Figure 2.4 Geometry of light from fiber.

Where G is Gaussian distribution of light emitting from tip of fiber, C is representation of geometrical spreading of light and $\Phi(z)$ accounts for absorption and scattering of light in tissue.

The Gaussian distribution of light $G(r, z)$ coming from the fiber [46] is given by

$$G(r, z) = \frac{1}{2\pi} \exp\left[-2\left\{\frac{r}{R(z)}\right\}^2\right] \quad (2.4.2)$$

$$\text{Where, } C(z) = (R_0 / (R(z)))^2$$

$$R(z) = R_0 + z \tan(\theta)$$

2.5 Monte-Carlo Modeling

Monte Carlo Modeling is stochastic method which can be used of light interaction with tissues .The models can be built such that increasing complexity can be added as the model develops. The simulations treat photons as neutral particles rather than as a wave phenomenon where photon are assumed to multiply during scattering in tissue [47]. During simulation process, the numbers of scattered, absorbed and transmitted photons are taken into account.

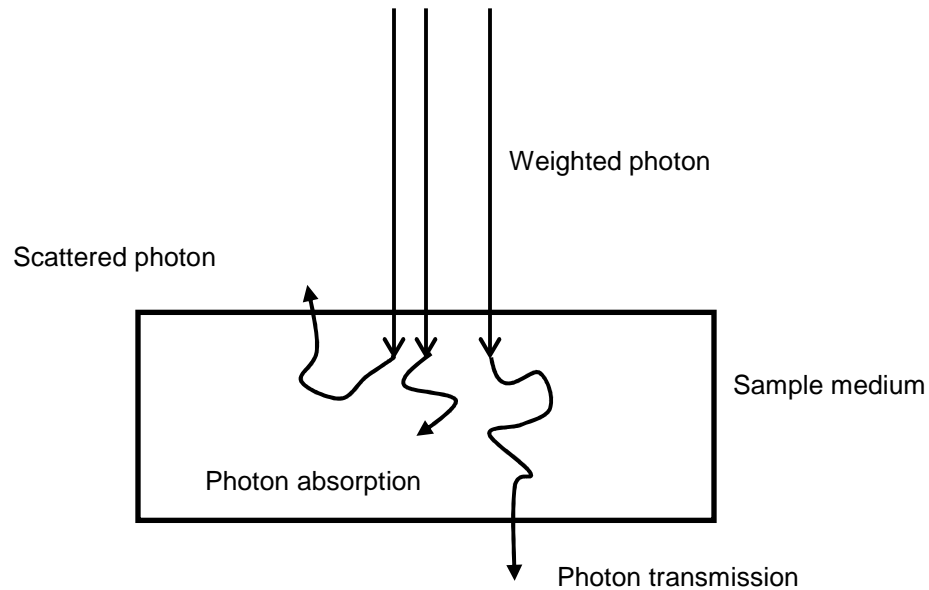


Figure 2.5 Geometry used for Monte-Carlo Simulation.

General equation used for the interaction of light in different layer of tissues having absorption coefficient and anisotropy is given by

$$I(z) = I_0 k \exp(-z/\delta) \quad (2.5.1)$$

Where $\Phi(z)$ is photon fluence and k is back-scattering [48] constant, which depends refractive index of the different layers in consideration and δ is the penetration depth given by,

$$\delta = \frac{1}{\sqrt{3\mu_a(\mu_a + \mu_s + (1-g))}}$$

μ_a = absorption coefficient

μ_s = Scattering Coefficient

g = anisotropy factor

Following are the steps involved in the MC simulation [48].

- Random Number Generation
- Attenuation of Collimated beam in Tissue
- Scattering of Photons in Tissue
- Anisotropic of Tissue
- Index Mismatch of Boundary Layers
- Grid Structure
- Finite Beam Width
- Multiple Layers
- Fluorescence
- Detector

Initially photon is weight of unity. The photon's interaction distance for the first step is found and photon is moved. The possibility of the internal reflectance is determined from numbers of photon left the tissue [49]. Photon position is determined if photon is reflected internally with program otherwise event is recorded as transmittance. Photon weight is determined in each step. The fraction of photon gives the energy absorbed by the tissue [50]. The boundary index is matched. Remaining photons are then randomly scattered in new direction and again new step is calculated and continued when photon weight is falls

below the threshold [48]. Flow chart of steps involves in simulation has been shown in Figure 2.6.

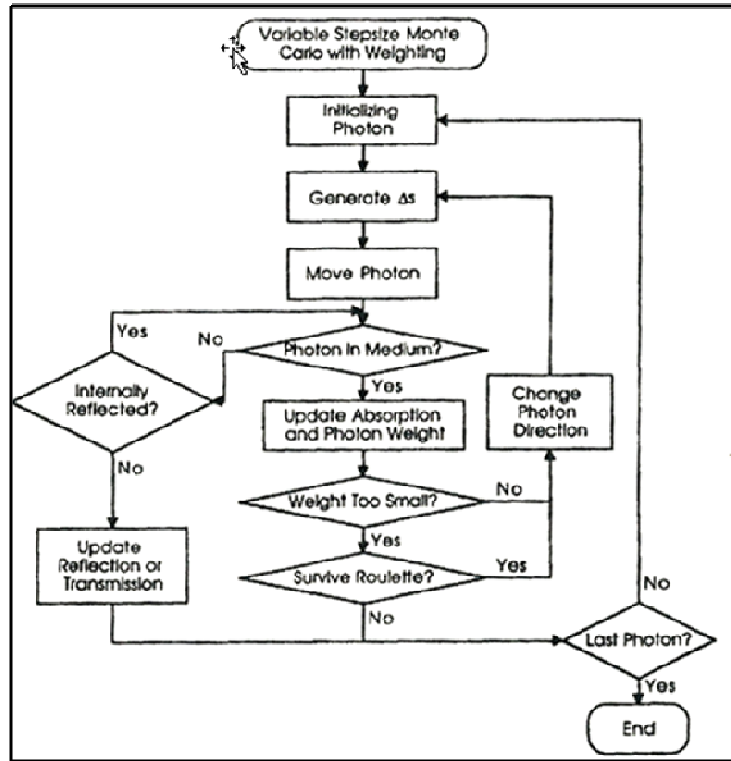


Figure 2.6 A flow chart showing simplified model of Monte-Carlo Simulation.

2.6 Stimulation theory

A simplified model of saturation-limited ChR2 activation by two-photon excitation (TPE) was applied as described in the previous study [39]. This model [39] describes only the transient photocurrent arising from a population of illuminated ChR2 molecules and assumed that the population of molecules was initially homogenous and in the excitable ground state. A ChR2 molecule with a 2-photon absorption cross-section σ_2 and illuminated with intensity $I(t)$, should absorb light at a rate $(\sigma_2/2)I(t)^2$. For this single-photocycle model, the concentration $p_g(t)$ of molecules in the ground state is given as [39]

$$\rho_g(t) = \rho_{g0} e^{-\frac{\sigma_m I(t)^m}{m} t}$$

where $m = 1, 2$ for single photon and two photon,

$$\rho_g(t) = \rho_{g0} e^{-\frac{\sigma_2 I(t)^2}{2} t} \quad (2.5.1)$$

where ρ_{g0} is the ground-state concentration at $t=0$. Considering the cell membrane to be in a plane, the ChR2-molecules are illuminated with a radially symmetric profile $I(r, t)^2$ as modeled from section 2.4. The rate of recruitment to a particular excited state with a population $N(t)$ is given by [39]

$$\frac{dN(t)}{dt} = \eta \frac{\sigma_m}{m} \int_s I(r, t)^m \rho_g(r, t) dA \quad (2.5.2)$$

where $m=1, 2$ for single-photon and two-excitation; η is the quantum efficiency; $\rho_g(r, t)$ having an explicit spatial dependence. $N^*(T)$, the number of current-conducting molecules at time $t = T$ after light onset, can be calculated by weighting the excitation rate with the channel's impulse-response function and integrating in time,

$$N^*(T) = \int_0^T \frac{dN(t)}{dt} [e^{-\frac{T-t}{\tau_2}} - e^{-\frac{T-t}{\tau_1}}] dt \quad (2.5.3)$$

where τ_1 denotes latency of molecules entering the current-conducting population after excitation and τ_2 denotes the characteristic decay time constant of these currents. Equation 2.5.3 gives the total number of ChR2 molecules excited under illumination. As ChR2 is non-specific cation channel, total current from single ChR2 molecule depends on the permeability of sodium, potassium and chlorine ions through the membrane [51].

Let G_{Na} , G_K and G_{Cl} be the conductance of respective ions and V_m is the membrane potential.

$$\text{Then, } I = V_m * G_{Na} + V_m * G_K + V_m * G_{Cl}$$

The instantaneous current is given by

$$I^*(T) = I * N^*(T)$$

Integrating equation 2.5.3 and neglecting the decay time (since we are only interested the maximum current which is produced during excitation),

$$N^*(T) = N_t \eta \left\{ \frac{\tau_1}{\tau_g - \tau_1} \left(e^{-\frac{T}{\tau_g}} - e^{-\frac{T}{\tau_1}} \right) \right. \quad (2.5.4)$$

where τ_g is the ground state life time, defined as $1/\sigma_1 I$ for single photon and $2/\sigma_2 I^2$

$$\text{Here, } I^*(\text{max}) = \eta * I * N^*(T)$$

In above equation 2.5.4, at any instant, T, and τ_1 are constant. We are interested to vary the intensity of light $t_g \sim 1/I_0^2$

Simplifying this equation,

$$I^*(\text{Max}) = I * \alpha * \eta * I_0^2 * (e^{-cI_0^2})$$

where I = Single channel ionic current

α = proportionality constant

C = constant

η = quantum efficiency

I_0^2 = Intensity profile.

This experiment was designed to study the variation of current with the increasing power density. All other parameters were kept constant at given time and intensity only was varied. The nature of this equation is non-linear with quadratic-dependence on intensity. However, our experimental data is linear. We hypothesize that the non-linear stimulation [52] may contain contributions from second harmonic generation (SHG) in the ATR molecule activating the ChR2 molecule via single-photon.

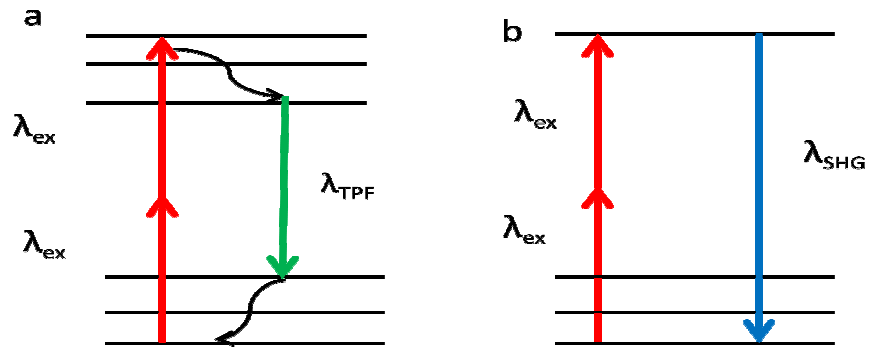


Figure 2.7 Schematic diagram showing difference between (a) two-photon fluorescence (b) second harmonic generation.

Second harmonic generation is a non-linear optical process in which multiple photons, interacting with non-linear material, combine to form a single photon. Evidently, in this study, the near infra-red light from the Ti:Sapphire laser was incident in the brain tissue or cells (non-linear medium) have higher probability to produce second harmonic generation with 25% efficiency which is blue light (single photon) in this case, [53] in such situation, only difference would be in single photon absorption cross section.

The combined effect due to two photon as well as second harmonic generation, the total current due to both effects in consideration is given by

$$I^*(Max) = I * \alpha * \eta * I_0^2 * (e^{-cd_0^2}) + \beta * I_0^2 \quad (2.5.5)$$

Where β is contribution from second harmonic generation.

As NIR light was used for two-photon excitation, we cannot disregard the possibility of photothermal effect since water has high absorption in NIR region. Temperature transients induce an inward transmembrane stimulation current which is proportional to their time derivative ($I \propto dT/dt$). Thus, The mechanism underneath neuron stimulation by NIR light is thought to be mediated by photo-thermal tissue transients, which can also potentially be induced using extrinsic absorbers (Photo-Absorber Induced

Neural-Thermal Stimulation or PAINTS) [54]. The reason underlying stimulation of neurons by near infrared light is yet to be understood however, recent research shows the mechanism is due to change in capacitance of neuron due to increase in temperature [62].

2.7 Channelrhodopsin-2 dynamics

Channelrhodopsin-2 (ChR2) is a light gated cation channel derived from the microbial *Chlamydomonas reinhardtii* algae [55]. ChR2 can be expressed in other biological cells including mammalian cells. Recent development in neuroscience have shown that the ChR2 can modulate the neuronal as well as cellular activity [56]. These types of opsins when genetically expressed to the specific cells can depolarize (channelrhodopsin-2) or hyperpolarize (halorhodopsin) [57] the cells evoking or inhibiting the action potentials in neurons when stimulated blue light by single photon stimulation or infra- red light by two-photon stimulation. Though ChR2 was widely used in biology, recently, in neuroscience research, numbers of questions are still remains unclear regarding the channel activation response and its complete photocycle. Several modified forms of the channel each encoded with single gene, have been expressed in excitable cells or neurons to alter its conductance [58]. The details photocycle of ChR2 is still unknown to the date, however, three or four state of photo cycle of ChR2 is widely used. Here, simple two-state (Figure 2.a) model of ChR2; open -state (O) and closed state (C) was assumed [59]. The opening and closing of ChR2 is on the scale of milliseconds [55], which is highly useful to study neuronal modulation and complex circuitry. The opening of ChR2 molecules is primarily due to conformational change of all-trans retinal (ATR). Upon shining the light, ATR changes from trans to cis structure which leads to the molecule opening [60]. The ATR molecule may also produce second harmonic generation (SHG) as shown in Figure 2.b [61].

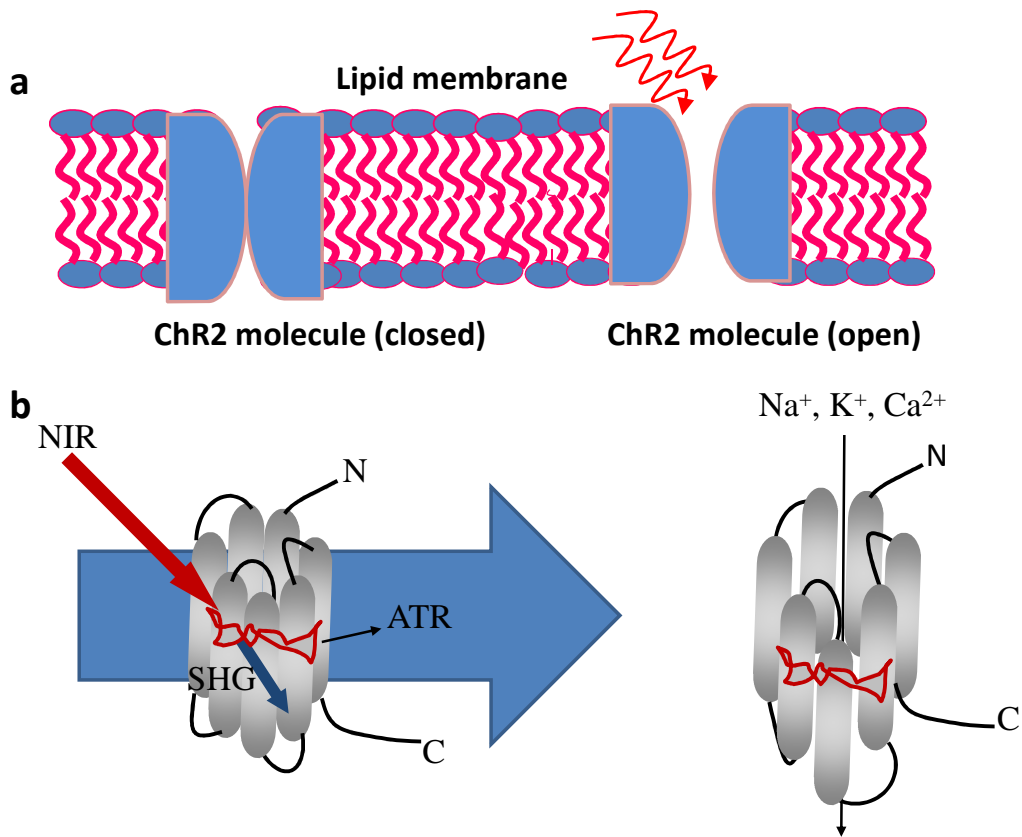


Figure 2.8 (a) Channelrhodopsin (CHR2)/light interaction and (b) conformational change of ATR, which leads to CHR2 opening.

Chapter 3

Materials and Methods

3.1 Cell culture

HEK 293 cells were transfected with the ChR2-EYFP construct, cloned into pcDNA3.1 neo (Invitrogen, USA). ChR2 cDNA was kindly provided by Dr. Georg Nagel (University of Wuerzburg, Germany). EYFP was fused in-frame to the C-terminus of ChR2 by PCR. Transgene-expressing cells were identified by visualizing the EYFP fluorescence under suitable illumination (514 nm). Stable clones were selected with 200 mg/l G418 and colonies were picked after 2 weeks, and then expanded. Clones that showed the highest level of EYFP fluorescence were chosen for the optical activation experiments. Cells were maintained at 37°C, 5% CO₂ in DMEM containing 10% fetal bovine serum. For generating light activation, cells were loaded with all-trans retinal (1 μM) for at least 6 hours and activated with fiber-optic laser beam.

3.2 Optogenetic stimulation

For both *in-vitro* and *in-vivo* activation of ChR2-expressing cells (identified by YFP fluorescence) or different brain regions expressing ChR2, both two-photon and single photon sources coupled to a 50 μm core optical fiber using a fiber coupler (Newport Inc.), mounted on a mechanical micromanipulator so as to position the tip of the fiber near the region of interest. The single-photon source consists of a blue (473 nm, 30 mW) diode laser coupled to the fiber, while the two-photon beam is provided by a 200 fs near-infrared Ti: Sapphire laser (Maitai HP, Newport-SpectraPhysics Inc.) beam operating at ~76 MHz, coupled to the same fiber. Further, the two-photon laser wavelength was tuned from 750 to 950 nm in order to compare the relative efficiencies of

the various NIR wavelengths. Macro-pulses of stimulation light were generated by a function generator driving the electro-mechanical shutter in the beam path. The function generator was synchronized to the *in-vitro* and *in-vivo* electrophysiology recording system (Plexon and Biopac Inc.). Light power at the fiber-tip was measured using a standard light power meter (PM 100D, Thorlabs Inc).

3.3 Patch-clamp recording

The opto-electrophysiology set up was developed on an Olympus upright microscope platform using an amplifier system as shown in Figure 3.1a. (Axon Multiclamp 700B, Molecular Devices Inc.). Parameters of the pipette puller were optimized in order to obtain desired borosilicate micropipettes of resistance from 3 to 5 M Ω for whole-cell patch clamp. Heat controlled method was used to make the glass electrode for patch clamp. Two-stage pipette puller was used from David KOPF's instrument as shown in Figure 3.1b.

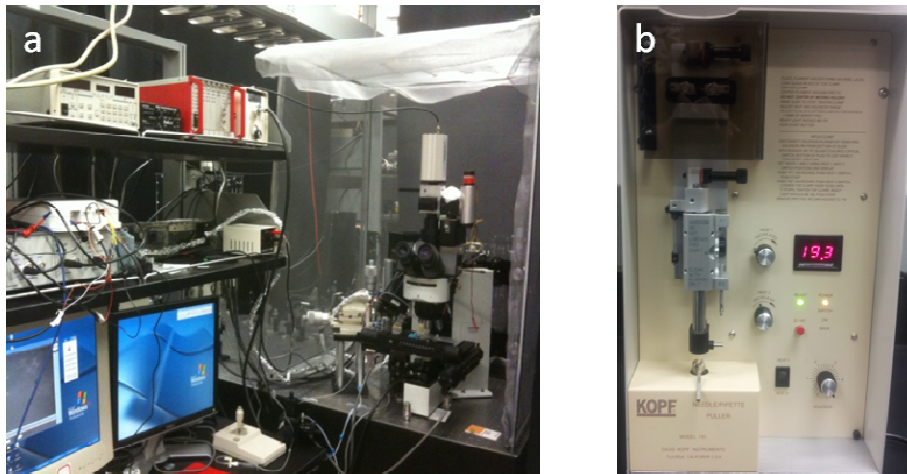


Figure 3.1 Laboratory set up for (a) *in-vitro* recording (b) two-stage micro-pipette puller.

The micropipette was filled with a solution containing (in mM) 130 K-Gluconate, 7 KCl, 2 NaCl, 1 MgCl₂, 0.4 EGTA, 10 HEPES, 2 ATP-Mg, 0.3 GTP-Tris and 20 sucrose. The electrode was mounted on a XYZ motorized micromanipulator (Newport Inc.).

standard extracellular solution containing (in mM): 150 NaCl, 10 Glucose, 5 KCl, 2 CaCl₂, 1 MgCl₂ was buffered with 10mM HEPES (pH 7.3). The output from the amplifier was digitized using a National Instruments card (PCI 6221). For electrophysiological recording, the hardware was interfaced with patch-clamp software from Univ. of Strathclyde (non-commercial use). Electrical recordings were performed at a holding potential of -60mV at room temperature (20-24°C). For activation of ChR2-expressing cells (identified by YFP fluorescence), the optogenetic stimulation beam (473 nm, or NIR) was delivered via a 50 µm core optical fiber, mounted on a mechanical micromanipulator so as to position the tip of the fiber near the desired cell being patch-clamped. For generating and controlling pulses of light, the electromechanical shutter in the laser beam path was interfaced with a PC. TTL pulses of desired frequency were generated using National Instruments (PCI 6221) card in order to generate required laser pulses for activation. For electrophysiological measurements subsequent to optical activation, the shutter was synchronized with the patch clamp recording electrode. The whole system was built on a vibration isolation table (Newport Inc.) and electrical isolation was done by means of a Faraday cage that was placed around the setup. pClamp software was used for data analysis.

3.4 Monte Carlo simulation

Monte Carlo simulation is known as the most reliable and flexible method for modeling photon migration in biological tissue. Here, Monte Carlo simulation codes for light propagation in multi-layered biological tissue named 'MCML'[48] and 'COV'[62] has been used in this study. The brain was modeled as two-layered tissue including grey matter and white matter. Parameters used for Monte-Carlo simulation were [63-65] (μ_a = absorption coefficient; μ_s = scattering coefficient; g = anisotropy factor; n = refractive index, and d = thickness of cortical layers) as listed in Appendix A for the simulation, and

then computed light propagation with the MCML code. Then the paired code 'COV' was utilized to extract the simulation output and calibrate the computed fluence rate distribution by quantitatively carrying the effect of Gaussian beam distribution and respective parameters, including beam size, laser power, and numerical aperture (NA). 10^7 photons were launched in each simulation to achieve an excellent signal-to-noise ratio in simulation output [48, 62].

3.5 Mouse preparation

The (Thy1-ChR2-YFP) transgenic mice, used in the reported experiments, were purchased from Jackson Labs. All aspects of experimental manipulation of our animals were in strict accordance with guidelines of the University of Texas at Arlington's Institutional Animal Care and Use Committee (IACUC). Mice were maintained on a 12:12 light cycle (lights on at 07:00)

3.6 *In vivo* optrode recordings

To validate opsin functionality in the mice, simultaneous optical stimulation and electrical recording in living mice was conducted as described previously [66], using an optrode composed of an extracellular tungsten electrode (1 M Ω , ~125 μ m) attached to an optical fiber (~200 μ m) with the tip of the electrode deeper (~0.4 mm) than the tip of the fiber to ensure illumination of the recorded neurons. Optical fiber was coupled to a 473 nm (for ChR2) laser (10 mW fiber output). Optrode recordings were conducted in mice anesthetized with xylazine and ketamine and the optrode was placed through craniotomies of size 400-500 μ m created above target regions. WinWcp and a NI DAQ board were used to both collect data and generate light pulses through the fiber. The recorded signal was band pass filtered at high 5000 Hz and low 300 Hz. For precise placement of the fiber/electrode pair, stereotaxic instrumentation was used.

3.7 In vivo electrophysiology recordings

Animals were deeply anesthetized with 90 mg/Kg ketamine and 10 mg/Kg xylazine and placed in a stereotaxic tool box. For *in-vivo* recording, a linear midline skin incision was made and burr holes were bilaterally drilled in the skull at the anteroposterior (AP) (in reference to bregma) and mediolateral (ML) coordinates corresponding to VTA (−3.2 mm AP; ±0.5 mm ML). The electrode was implanted stereotaxically to allow recording from deep brain regions. Continuous electrical activity was then recorded either via a multichannel acquisition system (Omniplex, Plexon Inc. and or via an amplifier (MP-150, Biopac Inc.) interfaced with the Acqknowledge acquisition software on a networked PC as shown in Figure 3.2

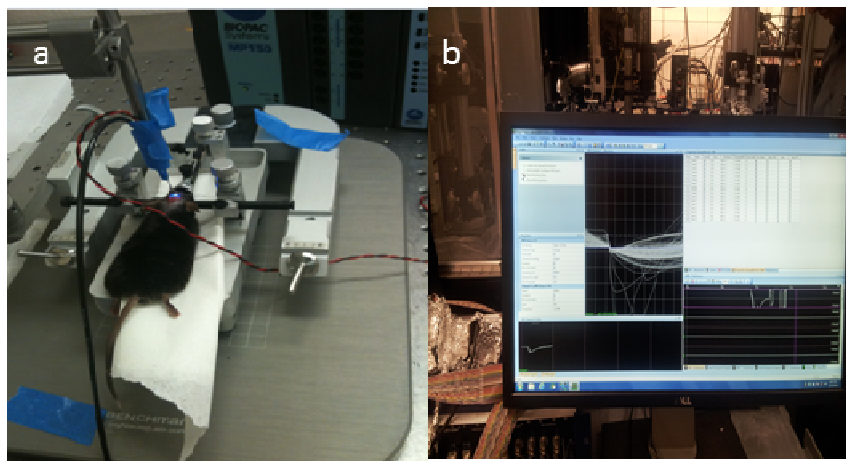


Figure 3.2 Laboratory set up for in-vivo recording (a) anesthetized mice in stereotaxic device (b) computer system (plexon Inc.) displaying in-vivo electrical activity.

3.8 Statistics

Data were analyzed using SPSS (IBM). One-way analysis of variance (ANOVA) followed occurred. The data were plotted as mean ± S. D. The accepted level of significance was $p < 0.05$. by Tukey's post-hoc test was used to determine whether a significant difference

Chapter 4

Results and Discussion

4.1 *In vitro* FO-TPOS irradiation leads to optogenetic stimulation

In contrast to the use of a microscope objective for focusing the two-photon laser beam, in this study a tunable (800 nm-900 nm), ultrafast (200 fs) fiber-optic beam was employed for two-photon optogenetic activation. In this case, similar to out-of-focus excitation [39, 43], diverging ultrafast fiber-optic near-infrared beam is believed to have sufficient photon densities to result in two-photon activation of the ChR2-transfected cells. For testing the efficiency of fiber-based two-photon activation in-vitro, HEK-293 cells expressing ChR2 were used and channel activities were recorded with patch clamp. The patch clamp set up for electrophysiological measurement subsequent to FO-TPOS is shown in Chapter 2. The tunable Ti: Sapphire laser (FSL, 76 MHz) was expanded using a beam expander (BE) and coupled to a fiber using a lens (L). A shutter (S) controlled the exposure (macro-pulse) duration and a circular neutral density filter (NDF) was used to control the average beam power. Expression of ChR2 in HEK 293 cells was confirmed by fluorescence imaging of reporter fluorescent protein (YFP). Figure 4.1a shows the bright field image of a patch-clamped HEK cell transfected with ChR2 and Figure 4.1b shows the YFP fluorescent images of HEK cells. Figure 4.1c shows raw recordings of inward current in response to five different randomly-selected macro-pulses (100 ms) of ultrafast (200 fs) laser pulses emanating from the fiber tip positioned 100 μm away from the clamped-cell resulting in a power density of $0.012 \text{ mW}/\mu\text{m}^2$. The current amplitude was similar to the current reported by previous microscope objective-based defocus laser spot study [39]. The fact that continuous wave (control) laser beam (operated in mode lock-off

condition), having same average power density (and exposure) did not induce inward current (Figure 4.1 c) confirms contribution of non-linear interaction of femto-second laser beam with the ChR2-expressing cells.

Cells were sub-cultured in Petridish. Before patching the cell, YFP fluorescent images were taken as shown in Figure 4.1b. The importance of this randomly selected macro-pulse in mode lock -off (continuous) and mode lock -on (pulsing) is to determine whether optogenetic stimulation was dominant or photothermal stimulation was also giving contribution to the inward current. If there was inward current in continuous laser stimulation, photothermal stimulation would be dominant.

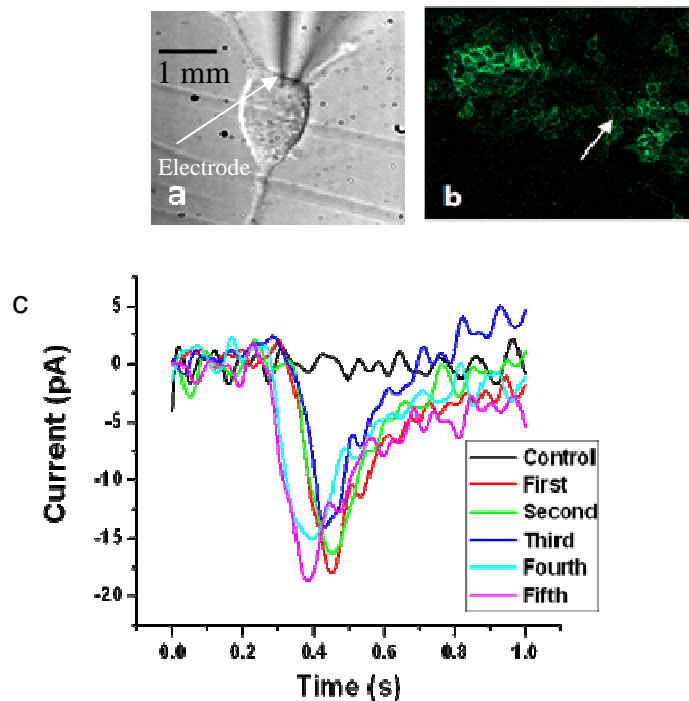


Figure 4.1 *In-vitro* two-photon activation of ChR2-expressing cells with ultrafast NIR laser beam: (a) Bright field zoomed image of a patch-clamped (marked by arrow) HEK cell transfected with ChR2, (b) YFP Fluorescence (marked by arrow) of HEK cells transfected with ChR2-YFP genes, (c) Inward current in response to macro-pulses (100 ms) comprising of ultrafast (200 fs) laser pulses.

In order to map the *in-vitro* fiber-optic two-photon activation spectrum of ChR2, the wavelength of the near-infrared stimulation laser beam was tuned from 800 nm to 900 nm. Figure 4.2a shows representative current responses recorded from a single cell, irradiated with ultrafast NIR laser beam (100 ms pulses, with average power density of $0.02 \text{ mW}/\mu\text{m}^2$, at cell membrane) at different wavelengths. The fiber-optic two-photon activation spectrum of ChR2 (Figure 4.2b) *in-vitro* shows that the peak activation wavelength is at 850 nm. Theoretically, two-photon optogenetic stimulation of cells is expected to be maximal near 900 nm-920 nm (double the single photon activation peak wavelength). The current amplitude at 900 nm was $9.9 \pm 0.6 \text{ pA}$ ($n = 18$), which was lower than the current amplitude at 850 nm ($28.0 \pm 2.4 \text{ pA}$, $n = 19$). The reason for this "blue-shifted" optimum stimulation wavelength for two-photon excitation with respect to single-photon excitation is similar to that observed [67, 68] in two-photon absorption of many fluorescence dyes. The observed blue-shift of the two-photon activation spectrum can be attributed to the parity selection rules favoring the two-photon activation of ChR2 (in closed form) to higher energy (open) state than the respective single-photon-induced activation. To produce a significant number of two-photon absorption events, the photon density must be approximately one million times that required to generate the same number of one-photon absorptions [69]. The consequence matches in mode-locked (pulsed) lasers, in which the power during the peak of the pulse is high enough to generate significant two-photon excitation.

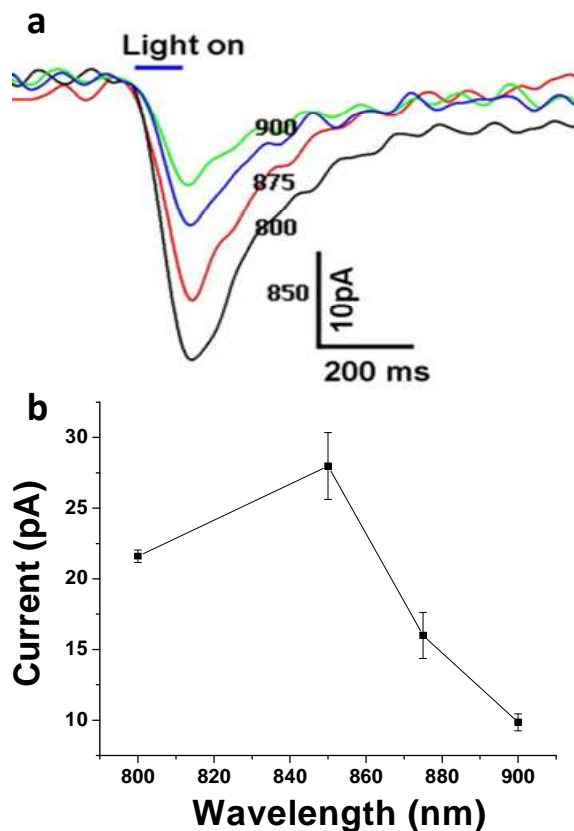


Figure 4.2 Current response due to control laser beam (operating in mode lock-off condition, i.e. continuous wave mode). (a) Representative current responses to ultrafast NIR laser beam at different wavelengths (b) Inward current responses due to fiber optic ultrafast stimulation (at 850 nm) using different power densities (in $\text{mW}/\mu\text{m}^2$; for $N=18$).

Since the peak of the two-photon activation spectrum was observed to be at 850 nm, this wavelength was selected for studying fiber-optic two-photon intensity-dependent current-response of cells. Figure 4.3 shows representative inward current responses due to fiber-optic ultrafast near-IR (850 nm) stimulation of a single cell at different average power densities ($0.006 \text{ mW}/\mu\text{m}^2$ to $0.02 \text{ mW}/\mu\text{m}^2$, at cell membrane). While highly non-linear response of inward current in low current regime (during focused irradiation) has

been reported earlier[70], the fiber-optic two-photon stimulation at higher laser intensities led to more linear dependence [52].

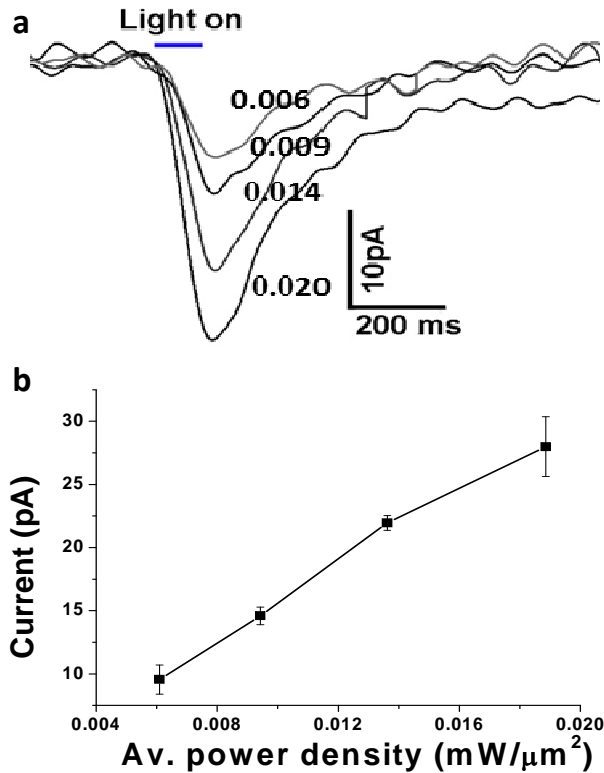


Figure 4.3 Peak amplitude of current with function of power density, (a) Fiber-optic two-photon activation spectrum at 0.02 mW/ μm² (100ms pulses) (b),dependence of inward-current as a function of power densities (at 850 nm, 100 ms pulses);for N= 6.

The dependence of two-photon (at 850 nm, 100 ms pulses) induced inward-current as a function of incident average power densities (near cell membrane) is shown in Figure 4.3b. Unlike two-photon fluorescence excitation, two-photon stimulation of ChR2 is not expected to have exactly quadratic intensity dependence due to the fact that in case of optogenetic activation, inward current is associated with conformational change of the molecule rather than a simple two-level transition as well as there is

possibility of second harmonic generation. Therefore, along with intensity, other parameters such as the kinetics of the opening of the ChR2-channel and two-photon absorption of all-trans-retinal [71, 72] will significantly modulate the nature of intensity- and wavelength-dependent current variations. It is important to note here that different scanning modes (spiral, raster) have also been applied for the excitation of ChR2-expressing cells to optimize the efficiency of excitation[39].

4.2 Peak FO-TPOS stimulation wavelength is also blue shifted

In order to achieve *in-vivo* two-photon stimulation of different brain regions of transgenic mice (Thy1-ChR2-YFP), fiber-optic delivery of the fs laser beam was employed instead of microscope objective. The schematic of single mode and multimode beam profiles for fiber-optic non-scanning two-photon activation is shown in Figure 4.4b. The fiber tip was placed in the cortical layer-1 of the transgenic mice and the electrode was translated stereotaxically to 1 mm beneath the fiber tip. In case of fiber-optic two-photon stimulation, the laser beam irradiates the entire cell(s), similar to the defocused beam used in the case of microscope objective. In the case of single mode fiber-optic beam, the intensity and, therefore, the two-photon stimulation is maximum at the center and slowly decays towards periphery (Gaussian nature). However, in case of the multimode fiber-optic beam, the maximum intensity spots are distributed over the irradiated cell(s) and two-photon stimulation is expected to occur in these spots (Figure 4.4b). Since these intensity-maxima are known to change their location in a random manner due to inter-modal coupling, self-scanning of the cell(s) by the mobile spots occurs.

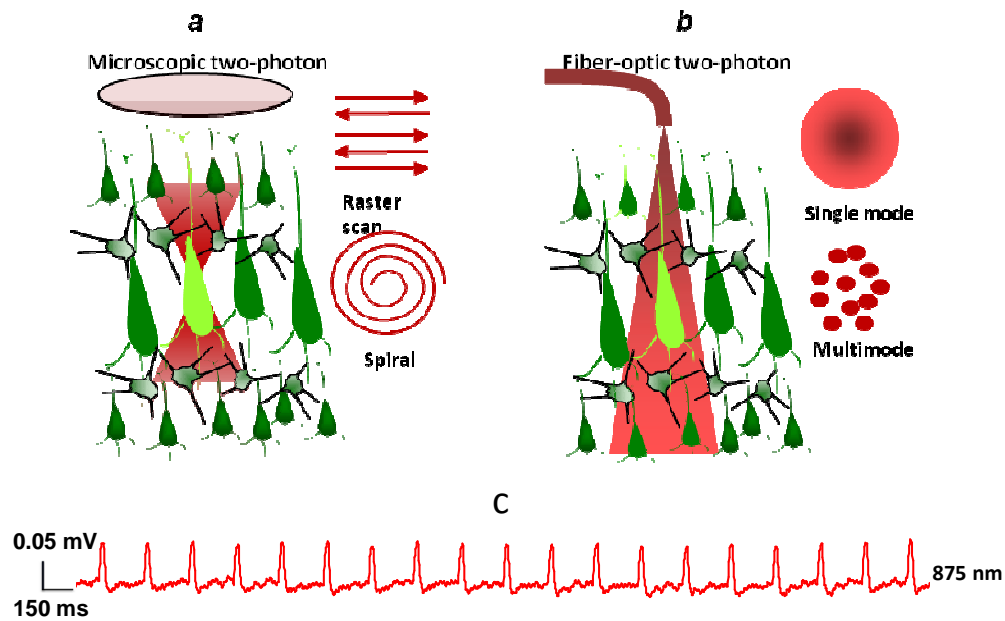


Figure 4.4 (a) Schematic of two-photon stimulation of targeted neuron with femtosecond laser delivered by objective. Also shown are two different scan patterns to generate action potential. (b) Schematic of fiber-optic two-photon activation by non-scanning defocused single mode and multimode beam profiles. (c) Raw spiking activity during in-vivo electrophysiology subsequent to fiber-optic two-photon optogenetic stimulation (FO-TPOS) at 875 nm (average incident laser power: $0.013 \text{ mW}/\mu\text{m}^2$, 5Hz).

In order to compare the relative efficiencies of various NIR wavelengths in fiber-optic two-photon optogenetic stimulation (FO-TPOS) in *in-vivo*, the (Ti: Sapphire) laser wavelength was tuned from 800 nm to 900 nm. The pump laser (Nd: YVO₄) beam power was controlled by varying the current driving the pump diode lasers so as to maintain equal power levels at different wavelengths. Figure 4.4c shows raw spiking activity recorded in cortical regions by *in-vivo* electrophysiology subsequent to fiber-optic two-photon optogenetic stimulation at selected wavelength (875 nm) with average incident laser power density of $0.013 \text{ mW}/\mu\text{m}^2$ (pulse width: 50 ms; frequency of shutter: 5 Hz).

Figure 4.5a shows variation of peak voltage as a function of in-vivo FO-TPOS wavelength. Though the in-vivo two-photon activation spectrum is of similar nature to that of the *in-vitro* patch-clamp experiments (Figure 4.2 and Figure 4.3), the slope was less steep towards higher activation wavelengths. At these NIR three wavelengths, the average power density of the fiber-optic beam was increased to $0.023 \text{ mW}/\mu\text{m}^2$, and spikes were recorded from the same site ($n=5$). Figure 4.5a shows an increase in peak amplitude of the recorded spikes at all the three wavelengths of *in-vivo* FO-TPOS for higher laser power density ($p<0.02$, $n=5$).

In order to further evaluate the efficacy of wavelength-dependent fiber-optic in-vivo two-photon activation, the firing rate (spikes per second) was measured and normalized (after subtracting number of background spikes, if any). Figure 4.5b shows the normalized firing rate as a function of wavelength of *in-vivo* FO-TPOS. In the case of two-photon firing-rate based activation spectrum, the wavelength-dependency is more favorable towards longer wavelengths as compared to the peak-amplitude (Figure 4.5a) and current based activation spectrum (Figure 4.2b). This may be attributed to differential absorption and scattering properties of neural tissue and water in the near-infrared region. While at longer wavelengths, the single-photon water absorption increases, the two-photon absorption of cellular chromophores and ChR2 is higher towards lower wavelengths. The fact that at higher wavelength (1000 nm), no significant stimulation was observed (data not shown) led us to conclude that contribution of direct (photothermal or photomechanical) stimulation is minimal. Further, these direct effects have earlier been found to occur at significantly higher pulse energies [73] and power densities [74] than that used in our current experiments.

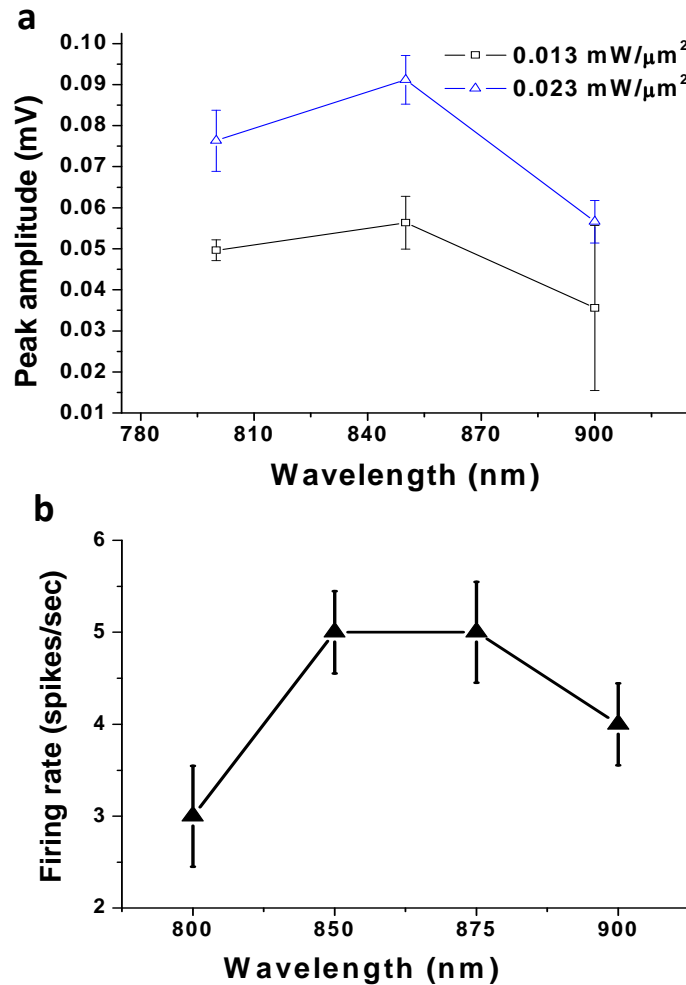


Figure 4.5 (a) Peak voltage vs. wavelength of *in-vivo* FO-TPOS at two different laser power densities, (b) Firing rate (spikes per second) vs. wavelength of *in-vivo* FO-TPOS for N=3.

4.3 *In vivo* FO-TPOS stimulation is intensity dependent.

To determine the variation of *in-vivo* two-photon activation efficacy as a function of average laser power density (intensity), the ChR2-expressing cortical regions of the transgenic mice were stimulated using the setup shown in Figure 2.3a. Further, to compare the intensity-dependency of *in-vivo* two-photon stimulation with that of single-

photon, a blue diode laser (473 nm) was combined with the two-photon laser beam using a dichroic mirror (DM), co-aligned by a folding mirror (M), expanded by beam expander (BE) and coupled to a single fiber using a lens (FL). A computer-controlled shutter (S) was used to control the stimulation pulse duration and the frequency of both the single and two-photon activation beams. In order to rule out photo-activation of the recording electrodes, which would lead to spurious signals, the optical fiber was affixed (shown by white line in Figure 2.3c) to a glass micro-pipette with the fiber-tip positioned ~1 mm ahead of the pipette tip. A tungsten electrode was inserted into the pipette containing extracellular recording solution ~2 cm away from the fiber tip. Loss of some near-infrared light from the fiber can be seen near the shank of the pipette tip due to bending of the fiber (Figure 2.3c). Figure 4.6(a) and (b) show recordings from the micropipette-electrode during ON and OFF cycles of ultrafast near-infrared irradiation with dry and wet electrode. The recording using the micropipette-electrode during *in-vivo* fiber-optic two-photon illumination of cortical region of deceased transgenic mouse brain is shown in Figure 4.6c. On the basis of all recording in Figure 4.6, the use of micropipette-electrode in combination with the light-delivery fiber being at fixed distance (1 mm) from the tip allowed us to remove the artifact (if any).

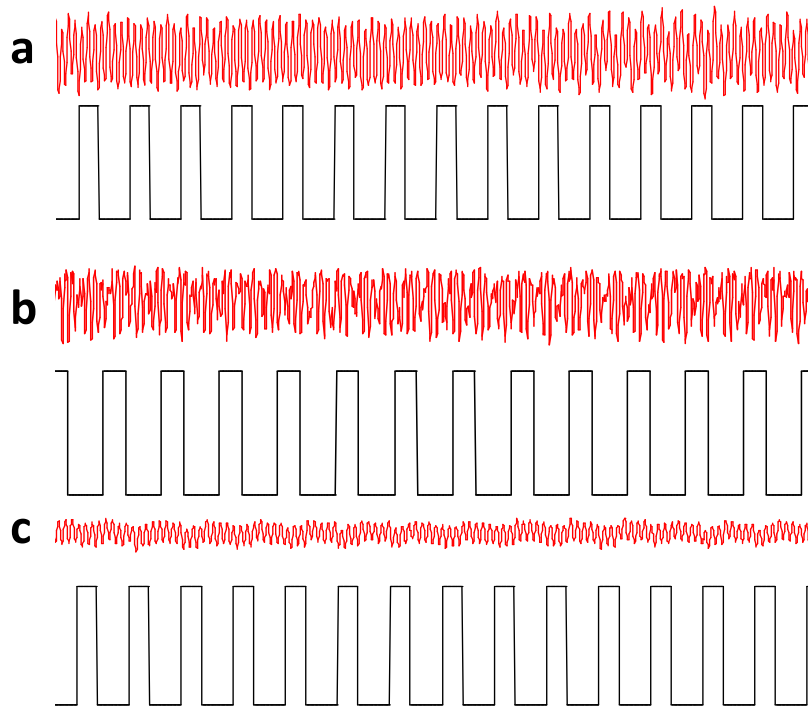


Figure 4.6 Direct two-photon illumination of micropipette-electrode separated by 1 mm (a) dry electrode (b) wet electrode. (c) Recording from micropipette-electrode during two-photon illumination one hour after death.

The micropipette-electrode-fiber carrying both blue and near-infrared laser beam was used to conduct an intensity-dependent comparison between single and two-photon in-vivo stimulation. Average incident laser power density was varied from ~ 0.006 $\text{mW}/\mu\text{m}^2$ to 0.026 $\text{mW}/\mu\text{m}^2$ for two-photon stimulation and that of single-photon stimulation was varied from ~ 0.0001 $\text{mW}/\mu\text{m}^2$ to 0.0008 $\text{mW}/\mu\text{m}^2$. Though the selected power-density range for two-photon activation is higher (~ 40 times) than that of single-photon, the phototoxicity data in cells shows that threshold average power density of near-infrared fs laser (810 nm) is ~ 1000 times higher than that due to continuous blue (458 nm) laser beam [75]. Two-photon activation at such low intensities is believed to be possible due to the large two-photon cross section of ChR2 [39]. The highest average

power density value ($\sim 2600 \text{ W/cm}^2$) for mode-locked near-infrared fiber-optic laser beam, used in the experiments reported here, is comparable to the reported [75] damage-threshold value of 1900 W/cm^2 for more-absorbing pigmented cells (with 250 ms exposure time). To further minimize damage in our intensity-dependent fiber-optic two-photon activation experiments, the pulse width of the shutter was set at 1 ms, thus resulting in a much lower dose than the damage threshold. In order to further ascertain that two-photon stimulation using such pulse-width (1 ms) is sufficient to generate spiking, the peak amplitude values were compared at three different pulse widths (1, 10, 50 ms).

In Figure 4.7a, it has been shown *in-vivo* raw spiking of locally stimulated ChR2-expressing cortical neurons (upper panel) of transgenic mouse in synchronization with two-photon stimulation (shutter opening: lower panel) at 870 nm. Figure 4.7b shows the variation of peak-amplitude as a function of pulse width for *in-vivo* FO-TPOS (870 nm) at two different average power densities ($0.013 \text{ mW}/\mu\text{m}^2$ and $0.017 \text{ mW}/\mu\text{m}^2$). While larger ($0.017 \text{ mW}/\mu\text{m}^2$) average power density led to higher peak amplitudes at same site of stimulation and recording ($p < 0.02$, $n = 5$), the variation of peak-amplitude with pulse-width was not significant ($n = 4$).

Figure 4.8b shows the peak-amplitude variation of recorded local electrical activity as a function of incident intensity of *in-vivo* FO-TPOS at two different wavelengths (870 nm and 900 nm) for same stimulation-detection sites ($n = 4$). The peak amplitude can be seen to increase with incident intensity for both wavelengths, but with a larger (2 times) slope for 870 nm than 900 nm. This intensity-dependent trend is not quadratic, similar to that observed in case of *in-vitro* experiments (Figure 4.3b). Besides the fact that conformational change of ChR2 upon two-photon irradiation is unlike excitation of fluorescent molecules, the *in-vivo* non-quadratic intensity-dependent behavior can also be attributed to higher number of neurons being recruited during increase in intensity.

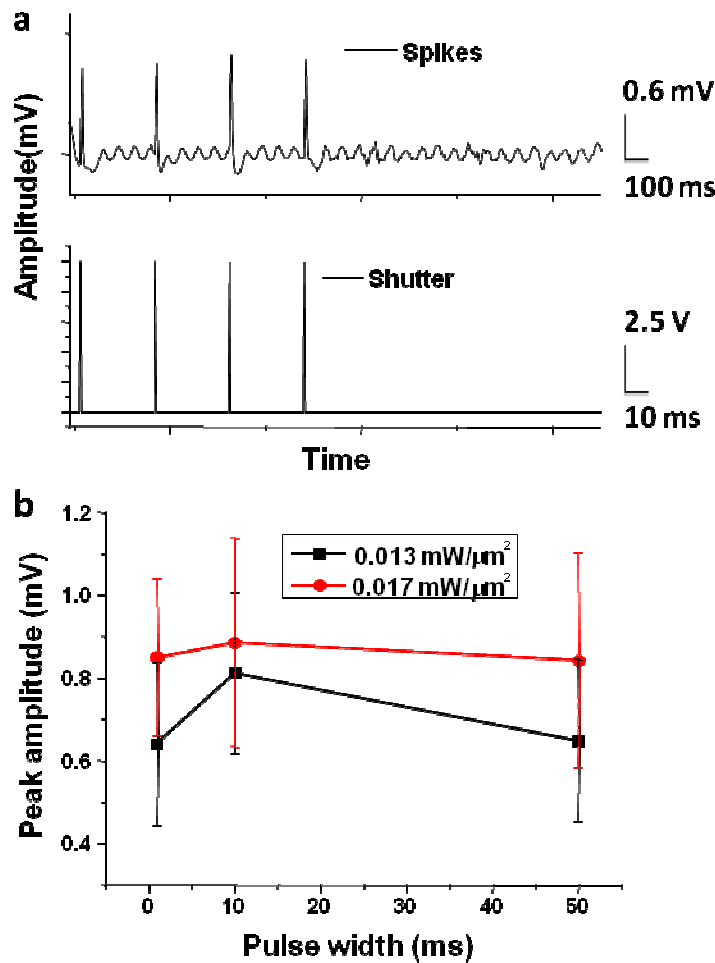


Figure 4.7 (a) *In-vivo* raw spiking of locally stimulated neurons (upper panel) corresponding to two-photon stimulation (shutter opening: lower panel) at 870 nm (b) Peak-amplitude as a function of pulse width of *in-vivo* fiber-optic TPOS (870 nm) at two different power densities; for N=3

The peak amplitude of single photon (473 nm)-activated neuronal firing as a function of power density is shown in Figure 4.8a. In contrast to *in-vivo* two-photon stimulation, the single-photon stimulation led to a saturation of peak amplitude at a threshold average power density of 3×10^{-4} mW/μm². This may be attributed to the fact

that unlike two-photon activation, most of the units near the vicinity of the recording electrode, contributing to the signal amplitude, are already stimulated within the excitable volume (limited depth) of the single photon beam. The red-shifted, one-photon stimulation is also expected to cause similar saturation behavior as a single-photon blue laser beam. The wide dynamic-range (Figure 4.8b) observed in the case of two-photon stimulation is advantageous in controlling the stimulation volume. This is owing to the non-linear nature of the two-photon activation process. When the stimulation power density increased from $0.0065 \text{ mW}/\mu\text{m}^2$ to $0.013 \text{ mW}/\mu\text{m}^2$, the firing rate of neurons also increased significantly ($p < 0.01$, $n = 6$).

Further, the stimulation might be possibility from photothermal stimulation since a temperature-rate current can easily derive from temperature-dependent changes in the membrane's capacitance. Such changes could result from rapid temperature-dependent changes in environmental pressure or in intra-membrane hydrophobic forces [76] which could both potentially lead to rapid membrane narrowing and thus a depolarizing current. Photothermal stimulation, path to light-mediated neuro-stimulation in various neural tissues may become possible due to high water-absorption in infrared region. Effective stimulation using this approach was demonstrated, for example, in peripheral nerves [77], cranial nerves [78], auditory [79] vestibular [80]), central auditory system *in vivo* [81] and *in-vitro* CNS neuronal preparation [82]. The three probable mechanisms for infrared neuron excitation are electric-field mediated excitation, photo-mechanical excitation and photo-thermal excitation, implying that the most likely mechanism is photo-thermal, resulting from the absorption of IR illumination by the tissue's water content.

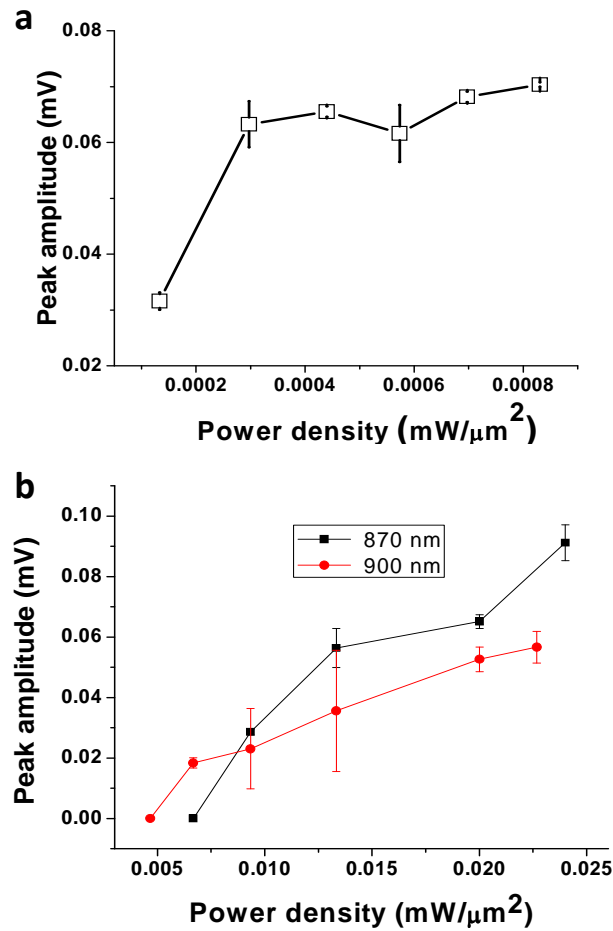


Figure 4.8 (a) Variation of peak amplitude of single photon (473 nm)-activated local electrical activity as a function of power density. *In-vivo* optogenetic stimulation using single (blue) vs. two-photon (NIR) stimulation. (b) Peak-amplitude of recorded local electrical activity as a function of incident power density of *in-vivo* fiber-optic TPOS at two different wavelengths; for N=3.

4.4 Comparison of depth penetration between two-photon and single-photon stimulation

In order to compare the efficacy of two-photon laser beam in stimulating depth brain regions *in-vivo*, with that of single-photon, this study first theoretically evaluated light propagation in the brain. Figure 4.9a shows the results of Monte Carlo simulations of

two-photon (870 nm) light propagation in the two-layered cortex for beam (diameter: 60 μm ; laser power: 5 mW) emanating from a fiber having numerical aperture (NA) of 0.15. Propagation of a single-photon (470 nm) fiber-optic beam for the same parameters (beam diameter, NA and laser power) is shown in Figure 4.9b. While it is evident that the near-infrared two-photon beam has a higher penetration depth (even at same power levels), this effect is more profound when (damage-threshold) normalized power levels are compared.

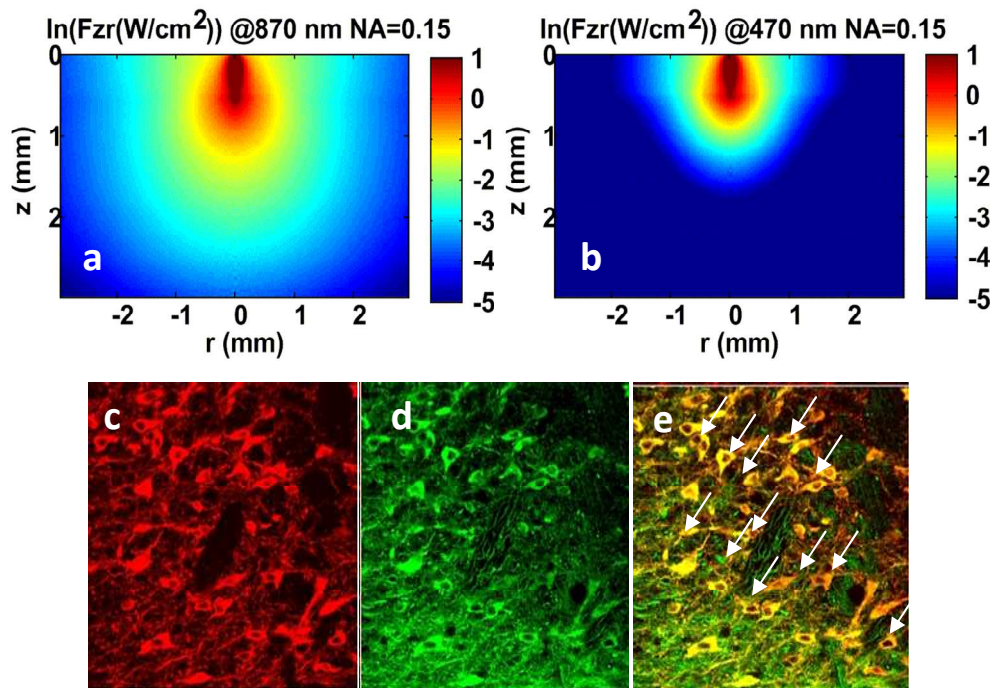


Figure 4.9 Monte Carlo simulation of light propagation in two-layered cortex for beam diameter of 60 μm , with laser power of 5 mW, (a) two-photon and (b) single-photon Gaussian beam. Confocal immunofluorescence images of a deep brain region of Thy1-ChR2-YFP transgenic mice. (c) YFP, (d) tyrosine hydroxylase (TH), (e) composite image. Arrows point to examples of colocalized YFP-ChR2 in dopaminergic neurons; for N=3.

To evaluate the ChR2-YFP expression in the targeted deep-brain regions of Thy1-ChR2-YFP transgenic mice, confocal immunofluorescence imaging of these regions was conducted. Mice were sacrificed after experiment and processed for brain slices. Figure 4.9c is the confocal image of brain slice from VTA region. This confocal image shows expression of reporter-molecule (YFP) at a depth of ~3 mm in the ventral tegmental area (VTA). As YFP is attached with ChR2, confirms that ChR2 is expressed in VTA region. Co-immunostaining for tyrosine hydroxylase (TH) and the composite images are shown in Figure 4.9d and Figure 4.9e respectively. The colocalization of tyrosine hydroxylase (TH) and ChR2-YFP is marked by arrows. Colocalization of tyrosine hydroxylase confirms the cells are dopaminergic cells. These results demonstrate that greater than 90% of YFP positive cells in the VTA of Thy1-ChR2-YFP transgenic mice were also positive for tyrosine hydroxylase (TH; Figure 4.9e).

Figure 4.10 shows MC simulation results depicting the effects of different parameters (power, NA, and wavelength) on light propagation in the two-layered cortex. For both FO-TPOS (870 nm) and fiber-optic single photon optogenetic stimulation (FO-SPOS) (470 nm), higher penetration depth was observed with increasing laser beam power (1 to 50 mW) as shown in the XZ-distribution of power density (W/cm^2) in Figure 4.10. In our experiments, ~50 times higher average power density was used in the case of FO-TPOS as compared to that of FO-SPOS. Therefore, when results of average laser beam power of 50 mW, in case of FO-TPOS is compared with 1mW of FO-SPOS, ~ 3 times higher penetration depth was observed in case of FO-TPOS for same fiber delivery geometry. Commonly used numerical aperture 0.3, 0.15 and 0.22 were taken in to consideration in our study. Variation of numerical aperture (NA) was independent for larger (1-3 mm) depth penetration. From the Figure 4.10 it is evident that NIR light has

higher penetration depth than visible blue light. This fact was employed to stimulate the ChR2 expressed neurons deep brain regions (~3mm).

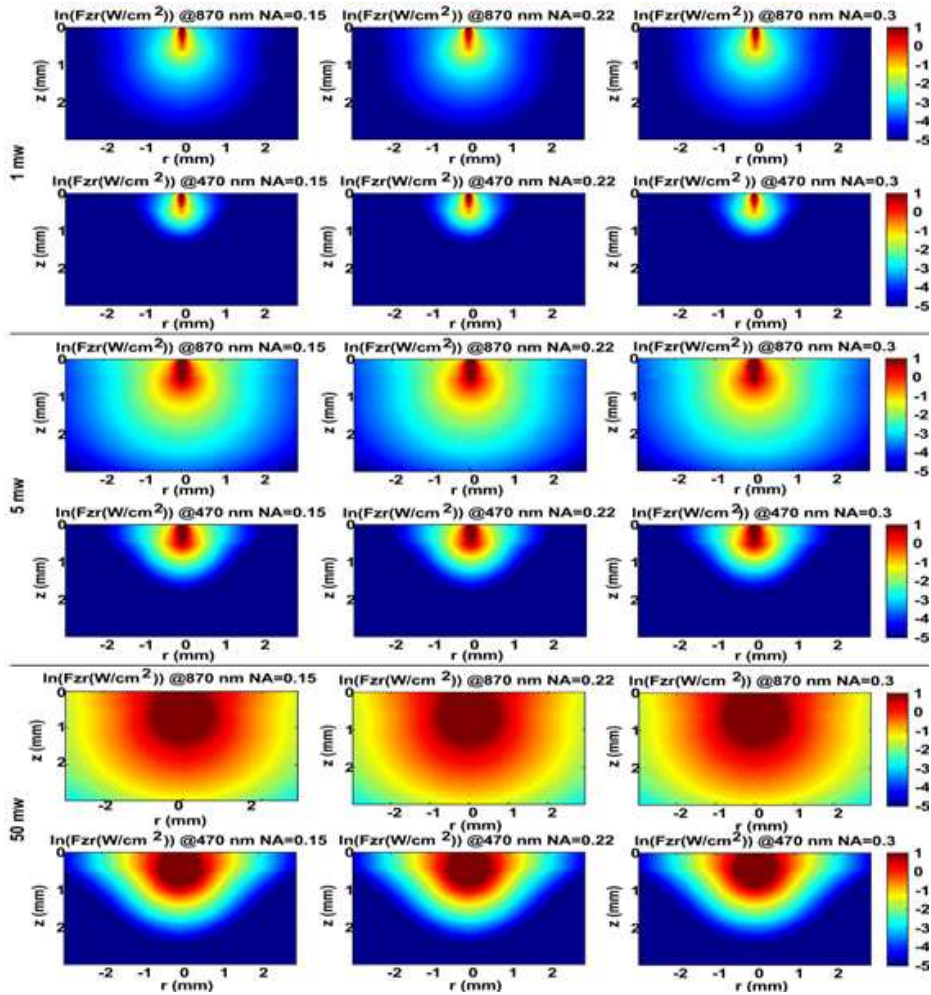


Figure 4.10 Monte Carlo (MC) simulation of light propagation in two-layered cortex for comparison of (a) fiber-optic two-photon optogenetic stimulation (FO-TPOS) vs (b) fiber-optic single-photon optogenetic stimulation (FO-SPOS). Effects of numerical aperture (NA) of optical fiber (0.15, 0.22, and 0.3) and laser beam power (1, 5, and 50 mW) on XZ-distribution of power density (W/cm^2) shown for near-infrared (870 nm) as well as blue (470 nm).

Next, in order to experimentally evaluate the depth activation efficacy of FO-TPOS in *in vivo* transgenic mouse models, with employed the set-up shown in Figure 2.3a, in chapter 2, with the electrode tip at varying axial distances from the stimulating fiber-tip. The fiber tip was placed in cortical layer-1 of the transgenic mice with the electrode being translated stereotaxically to different depths of the brain.

In contrast to two-photon activation, no spiking signal was observed at large depths (3 mm) when single-photon beam was used for stimulating the same sites as used for two-photon. Comparison of single and two-photon activated depth-dependent spike-amplitude is shown in Figure 4.11a. It was observed that even in the first layer of the cortical layer (~1 mm from the dura) peak amplitude of two-photon activation is greater than the single photon which is due to saturation effect in single photon. All the molecules in the volume of excitation get stimulated during the single photon stimulation hence current reaches soon maximum and saturated unlike two photon excitation, it has been shown the significant variation of peak amplitude of two-photon (850 nm) activated local electrical activity as a function of depth at different power densities ($p < 0.001$, $n = 5$). As depth increased, blue light (single photon) scattered and absorbed sharply since scattering is inversely proportional to the square of the wavelength. Blue light has smaller wavelength (470 nm) than the NIR light (875 nm in our case). Further, blue light get attenuated fast in the tissue. Thus, in the greater depth > 1 mm, blue light could not produce action potential due to lack of threshold photon density. This is also verified my Monte Carlo simulation.

Raw spiking local electrical activity is shown in Figure 4.11b. Clearly distinguishable action potentials were observed up to depth ~2 mm. Noticeable local electrical activity was observed up to ~3 mm as shown in Figure 4.11b.

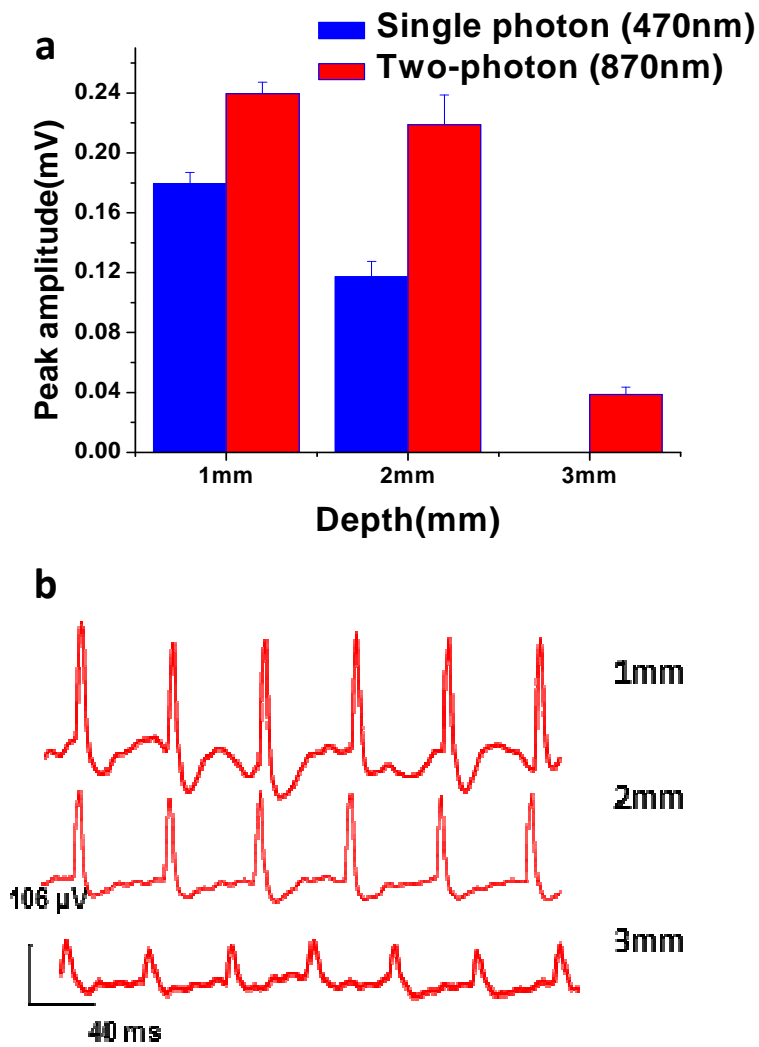


Figure 4.11 (a) Raw spiking activity at different depths due to *in-vivo* fiber-optic two-photon optogenetic stimulation (FO-TPOS). (b) Comparison of single and two-photon activated depth-dependent peak amplitude; for N=3.

Figure 4.12a shows variation of peak amplitude as the function of depth in different laser power densities. While increasing the depth, peak amplitude was decreased for a given power but the value was higher for higher power densities. Similar nature of graph was obtained for various power densities.

Figure 4.12 b shows comparison of peak-amplitude at different depths due to *in-vivo* FO-TPOS for two different wavelengths (850 and 870 nm) at same average power density ($0.024 \text{ mW}/\mu\text{m}^2$). For all the power densities, while there is no significant decrease in peak amplitude from 1 to 2 mm. Significant ($p < 0.001$, $n=5$) decrease in signal amplitude was observed when moving from 2 to 3 mm depth.

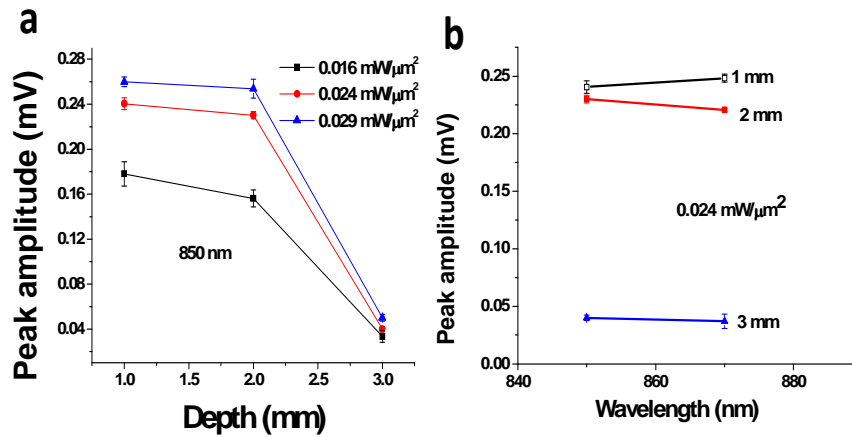


Figure 4.12 (a) Variation of peak amplitude of FO-TPOS as a function of depth at different power densities. (b) Comparison of peak-amplitude at two different wavelengths of *in-vivo* FO-TPOS at different depths; for $N=3$.

Similar depth-dependent variation of peak amplitude was observed for 870 nm in Figure 4.13a, and 900 nm in Figure 4.13b at different power densities. This is true for all the near-infrared wavelengths reported here. Further, the decrease in peak amplitude as depth increases is sharper in 900 nm than in 870 nm. This sharp decrease may be attributed as photothermal stimulation. In this study absorption peak of two-photon optogenetic stimulation was characterized and found to be maximum in 875 nm *in-vivo* and 850 nm in *in-vitro* as shown in earlier Section 4.1 and Section 4.2.

As we go further in NIR region the probability of getting photo thermal stimulation is higher. In photothermal stimulation, rise in transient temperature is maximum in the vicinity of the point of light interaction [83]. As fiber is placed in the first cortical layer, rise in transient temperature due to laser pulse occurs at the layer and might propagate at proximity of first layer. Possibility of direct photothermal stimulation at greater depths (~2-3mm) is minimum since heat is lost rapidly due to thermal equilibrium. However, indirect stimulation at larger depths is possible and needs further investigation.

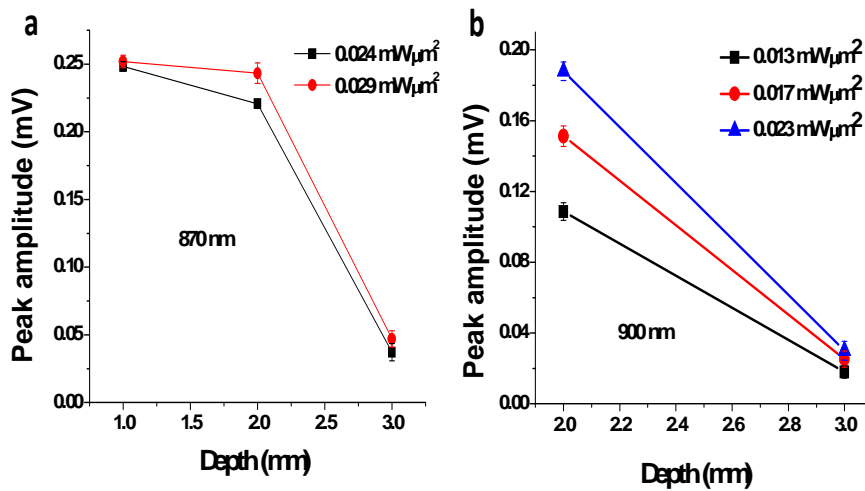


Figure 4.13 Variation of peak amplitude of two-photon activated electrical recording as a function of depth at different power densities (a) 870 nm, (b) 900 nm ;for N=3.

Histogram of peak amplitude as function of power densities at depth 1 mm, 2mm and 3 mm as a function of power density is shown in Figure 4.14a and Figure 4.14b at 850 nm and 870 nm which shows the similar nature as explained in Figure 4.12 and Figure 4.13.

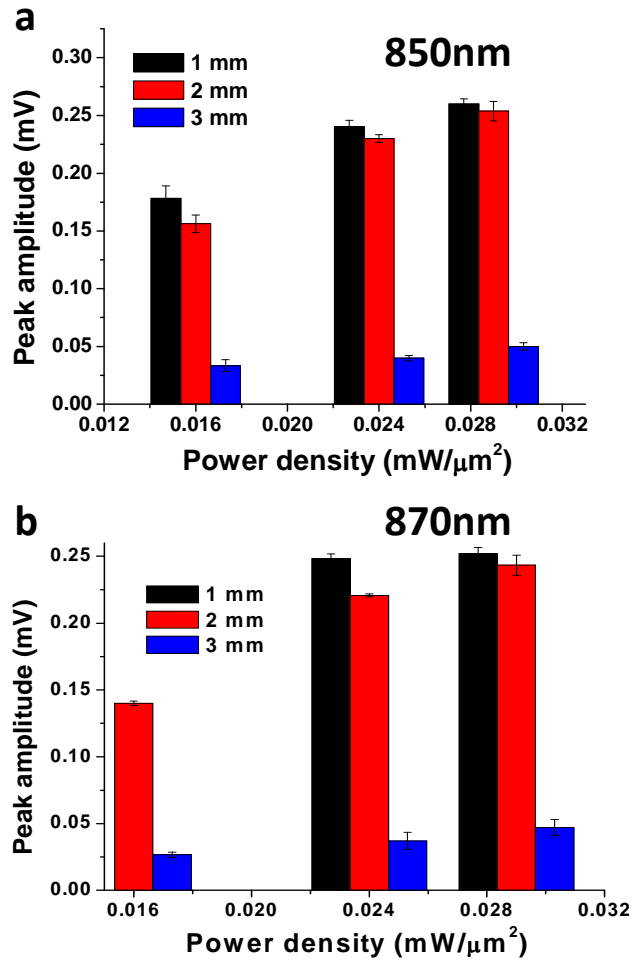


Figure 4.14 Histogram of peak-amplitude as a function of power densities of *in-vivo* fiber-optic (a) TPOS at different depths. (a) 850 nm, (b) 870 nm; for N=3.

4.5 FO-TPOS is direct stimulation

To verify whether fiber-optic two-photon beam can directly stimulate neurons *in-vivo* at large depth, analysis of FO-TPOS evoked spike latency (from the onset of light) at different depths from fiber-tip was carried out. The experimental setup in Figure 2.3a was used to compare the latency values for two-photon with that of single-photon. Figure 4.15a and Figure 4.15 b show schematics of depth stimulation limit of fiber-optic single-

photon and two-photon beam respectively. In single photon and two-photon stimulation modalities, both direct and indirect (post-synaptic) stimulations of neurons at different cortical layers (marked by blue line in Figure 4.15 a & Figure 4.15b) is possible. For single-photon stimulation, since the blue light is attenuated within 1mm of propagation in cortical tissue (Figure 4.10), it is suspected that the spikes from 3mm depths are mostly due to indirect stimulation. However, at depth of 3mm from the fiber-tip, no detectable signal was observed (Figure 4.15e) in case of blue-light stimulation (473 nm, 4 mW). In contrast to this, two-photon near-infrared beam has penetration depth of ~ 3 mm and therefore can directly elicit action potentials in neurons at larger depths (2-3 mm) along with the indirect post-synaptic spikes. Figure 4.15c shows the schematic diagram of mice brain showing VTA (marked by blue color) with reference to bregma. Raw electrical recording at 3mm depth for two-photon (870nm, 80mW) stimulation is shown in Figure 4.15d. In order to estimate the latency of the spikes evoked by FO-SPOS and FO-TPOS at different depths, very short (1 ms) stimulation pulses were used for these experiments and the raw spikes were overlaid with the shutter-synchronization pulses.

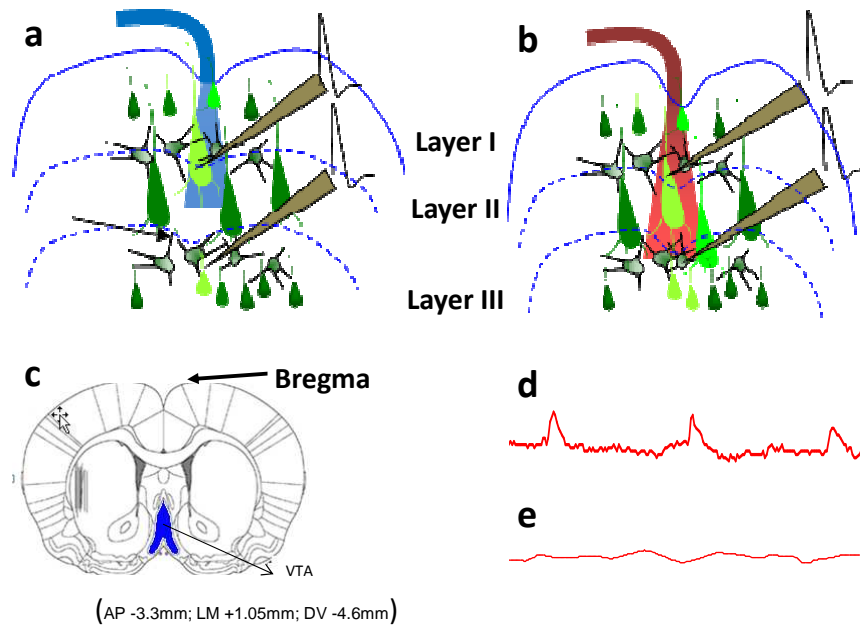


Figure 4.15 Sketch showing depth stimulation limit of fiber-optic. Different cortical layers are marked by blue lines (a) blue (single-photon) vs. (b) NIR (two-photon) light. (c) Representation of VTA region in mice brain with reference to bregma . Raw electrical recording at 3mm depth for (d) two-photon (870nm, 80mW) (e) single photon (470nm, 4mW) and stimulation.

Figure 4.16a shows the overlay of raw spikes (red profiles) with shutter (FO-TPOS ON) opening (black profiles) at different depths for two different wavelengths (850 nm and 870 nm). The comparison of values for spike latencies at different depths stimulated by single photon (473 nm) and two-photon (870 nm) fiber-optic beams is shown in Figure 4.16b. Though the mean value of spike latency increased with increasing depth for FO-TPOS, it was not statistically significant and therefore should have primarily originated from direct stimulation. The slight increase can be attributed to the contribution from spikes generated by indirect stimulation [84]. However, the statistically significant ($p < 0.001$, $n=5$) increase in latency values of spikes from 2 mm depth as compared to 1

mm depth in case of FO-SPOS (Figure 4.16b) indicates that most of the spikes are generated by post-synaptic cortical circuitry rather than direct stimulation by the blue laser beam. To check if latency is wavelength-dependent, Comparative studies using three different FO-TPOS wavelengths (850, 870 and 900 nm) was carried out.

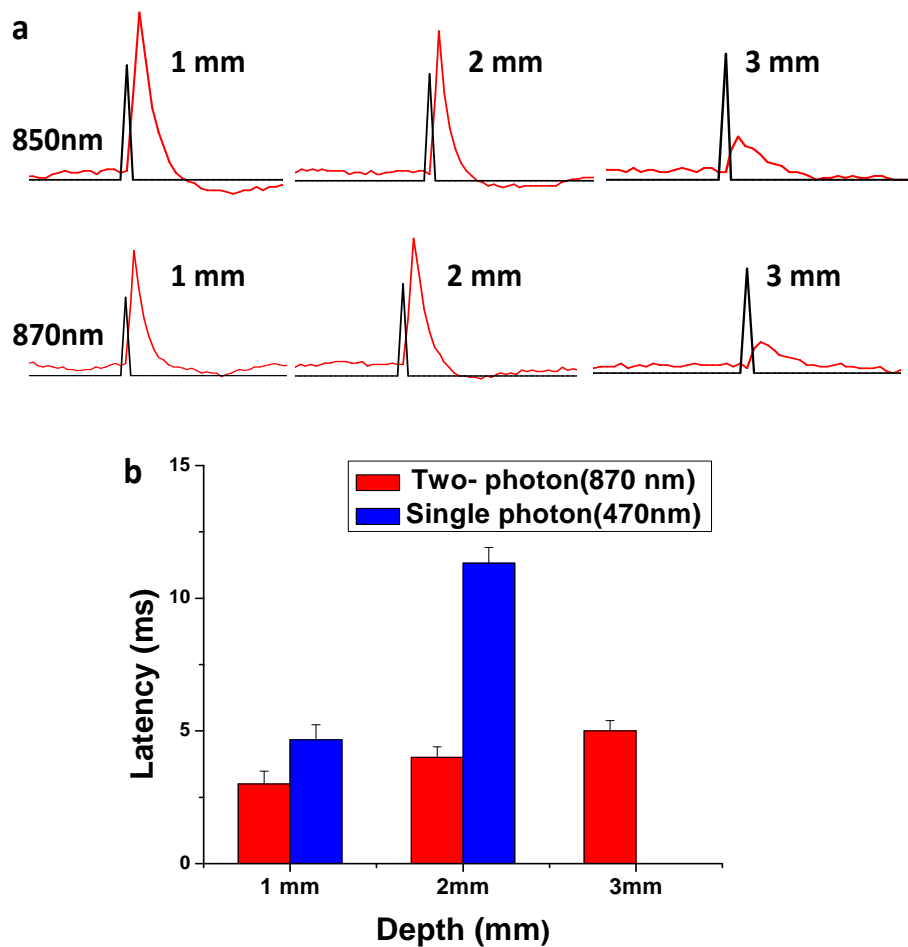


Figure 4.16 (a) Overlay of raw spikes (red profiles) with shutter (fiber-optic two-photon stimulation ON) opening (black profiles) at different depths for two different wavelengths. (b) Comparison of latency of spikes at different depths stimulated by single photon and two-photon (870 nm) fiber-optic beams ;for N=3.

There is no statistically significant variation of latency as a function of wavelength.

wavelength.

Figure 4.17a shows the histogram of latency of spikes at different two-photon wavelengths for three depths (1, 2 and 3 mm). The latency at 900 nm was slightly higher than that due to other two wavelengths, but statistically insignificant. Further study to understand the effect of average power density on the latency of two-photon (870 nm) evoked spikes was carried out. The variation of latency values as a function of depth for three different two-photon average power densities is shown in

Figure 4.17b. All the mean latency values are below 6 ms, implying direct stimulation [85]. While there is a slight increase in latency values at 3 mm depth, it is not statistically significant and may be attributed to some contribution from post-synaptic spiking.

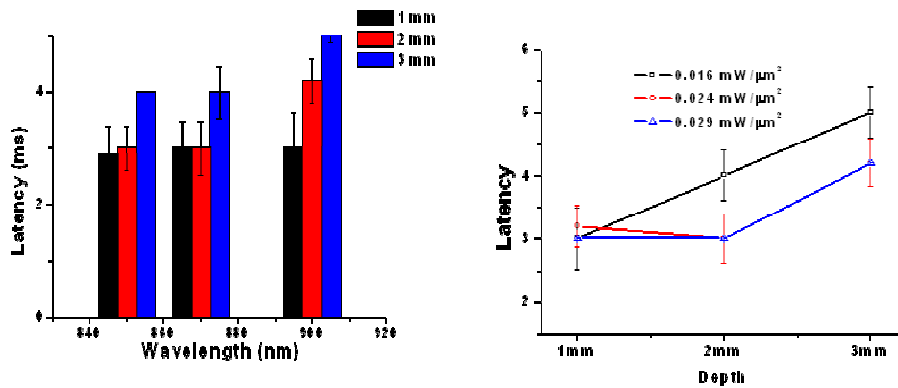


Figure 4.17 (a) histogram of latency of spikes at different two-photon wavelengths for three depths. (b) Variation of latency as a function of depth for different two-photon (870 nm) power densities ;for N=3.

Chapter 5

Conclusions and Future Work

5.1 Conclusions

The two-photon activation method reported here enabled in-vivo optogenetic stimulation up to depth of 3 mm in the brain. Thus, the fiber delivering the FO-TPOS beam could be positioned in superficial cortical layer, leading to minimal invasion into the brain. Though it has been characterized two-photon activation efficacy at different near-infrared laser parameters (intensity, exposure, wavelength etc), further studies are required to optimize the fiber-optic two-photon stimulation strategy. For example, the large (260 ± 10 GM) two-photon cross-section of ChR2 [39] should allow use of nanosecond or even microsecond compact near-infrared (NIR) sources for FO-TPOS.

Defocused fiber optic two-photon beam will cause minimal photo damage while stimulating the cells. The threshold average power required in generating action potential in the ChR2-transfected cells using defocused fiber beam is lower than that used for microscopic-objective two-photon stimulation. The TPS mediated sub-threshold stimuli can induce action potentials and can be used to selectively stimulate larger (100 μ m-motor neuron) cells which have lower thresholds than smaller (4 μ m- granule cell) cells. The fiber-optic method employed in this study is less-invasive since it can stimulate deep brain region from ~3 mm above the region unlike single photon, where optical fiber have to inserted in close proximity of the stimulated region. For example, in our study we have successfully stimulated VTA (~3mm) from the upper cortical layer (Dura as reference). The efficacy of fiber-optic two-photon stimulation was found to depend on the pulse width of laser, power density and excitation wavelength.

5.2 Future work

This non-linear optogenetic approach, combined with electrophysiology and behavioral readout(s), will provide a unique opportunity to dissect the functional neuronal circuitry of deep brain regions. The efficacy of the two-photon beam can be further improved by controlling the divergence of the beam emanating from the fiber. Since the two-photon process is non-linear in nature, focused near infrared activation can lead to highly localized activation of the specific region of interest, which may be located deep in the ventral portion of the midbrain. Our previous studies (both experimental and Monte Carlo simulation [86-88]) show that a non-diffracting optogenetic Bessel beam is more effective for depth stimulation than a classical (Gaussian) beam [89]. Figure 5.1 shows the comparison of microscopic two-photon setup with defocused and focused fiber-optic two-photon optogenetic stimulation.

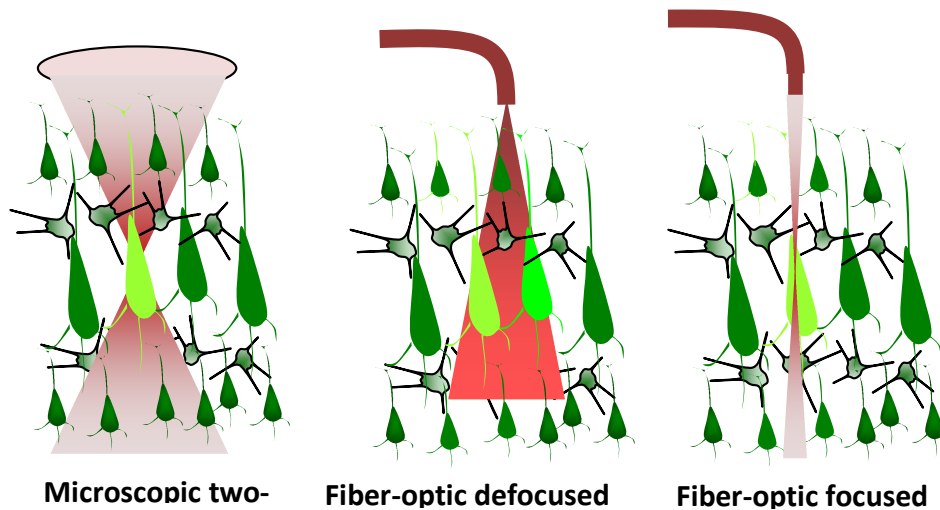


Figure 5.1 Comparison of microscopic two-photon setup with defocused and focused fiber-optic two-photon optogenetic stimulation.

For *in-vivo* two-photon activation, use of an axicon tipped fiber [90] will allow generation of Bessel beam for even better penetration. The propagation distance of the stimulating Bessel beam and the stimulation volume can be controlled by the cone angle of the fiber

tip. The use of the non-diffracting ultrafast Bessel laser beam for FO-TPOS of excitable cells will allow minimally invasive stimulation with improved spatial resolution. This can significantly enhance previous work using single-photon technology for mapping neural circuitry. Further, evaluation of ns and μ s pulse stimulation can be studied. In this research, simple two state photocycle activation of ChR2 molecule (open and closed) was modeled just to measure the maximum current during activation. However, multiple photocycles of ChR2 have been reported recently. Three or four state of ChR2 activation photocycle would provide better understanding in future.

Further, by characterizing the two-photon light activation spectrum for other opsins such as NpHR (chloride channel), the *in-vivo* FO-TPOS method can be used for inhibiting neural activity. In addition to the demonstrated depth stimulation capability of FO-TPOS, high spatial precision in two-photon optogenetic activation should be possible *in-vivo*, by virtue of non-linear nature of ultrafast light-matter interaction. Manipulation of deep brain regions via FO-TPOS as demonstrated by us, will lead to better understanding of neural circuitry because the technology permits noninvasive and precise anatomical delivery of light.

Another area of future work would be to alter the existing opsins by mutation and tune the different capabilities. Mutation of the residues in opsins by various methods [91, 92] have been started to observe the altered kinetics and its activation spectrum. It would be better if we could develop mutated opsins which have strong two-photon absorption cross-section in the near infrared spectrum. This would lead to minimize the requirement of very high photon density laser source such as laser. Thus, more affordable and compact ns or even μ s NIR laser sources may be used for two-photon stimulation.

Use of two-photon stimulation for activating halorhodopsin would be useful for localized silencing of the optogenetically-sensitized cells. Expressing ChR2 and

halorhodopsin together in the same cell can modulate its function more effectively than the case when only one protein is expressed. These two proteins act as “traffic light”. Channelrhodopsin-2 helps to initiate action potential whereas halorhodopsin inhibits the signal (action potential). Near infrared (two-photon) interaction of these proteins would lead to control of brain activities in behaving animal in a minimally invasive way.

Coupling optogenetic stimulation with other methods of imaging such as calcium imaging [93] would help in minimally-invasive study of neuronal circuitry. Voltage sensitive [94] dyes can be used to monitor electrical activities in cells during two-photon optogenetic stimulation. Biophysical characterization of ChR2 using Raman spectra, FTIR, NMR spectroscopy [95] coupled with X-ray diffraction can lead to better understanding of complete characterization of opsins including their kinetics.

Appendix A

Parameters of Monte-Carlo Simulation

Wavelength	Layer	μ_a (mm ⁻¹)	μ_s (mm ⁻¹)	g	n	d (mm)
470 nm	Grey matter	0.4	10.3	0.87	1.36	0.5
	White matter	0.36	43	0.78	1.38	2.5
870 nm	Grey matter	0.02	7.5	0.90	1.36	0.5
	White matter	0.06	31	0.88	1.38	2.5

References

1. Crick, F.H.C., *Thinking About the Brain*. Scientific American, 1979. 241(3): p. 219-&.
2. Seung, H.S., *Reading the Book of Memory: Sparse Sampling versus Dense Mapping of Connectomes (vol 62, pg 17, 2009)*. Neuron, 2009. 63(1): p. 139-139.
3. Hama, H., et al., *Scale: a chemical approach for fluorescence imaging and reconstruction of transparent mouse brain*. Nat Neurosci, 2011. 14(11): p. 1481-8.
4. Fenno, L., O. Yizhar, and K. Deisseroth, *The Development and Application of Optogenetics*. Annual Review of Neuroscience, Vol 34, 2011. 34: p. 389-412.
5. Nagel, G., et al., *Channelrhodopsin-2, a directly light-gated cation-selective membrane channel*. Proc. Nat. Acad. Sci., 2003. 100(24): p. 13940-13945.
6. Boyden, E.S., et al., *Millisecond-timescale, genetically targeted optical control of neural activity*. Nat Neurosci, 2005. 8(9): p. 1263-1268.
7. Nagel, G., et al., *Light Activation of Channelrhodopsin-2 in Excitable Cells of Caenorhabditis elegans Triggers Rapid Behavioral Responses*. Curr. Biol., 2005. 15(24): p. 2279-2284.
8. Christopher, R.B. and C.M. Cameron, *Role of electrode design on the volume of tissue activated during deep brain stimulation*. Journal of Neural Engineering, 2006. 3(1): p. 1.
9. Butson, C.R. and C.C. McIntyre, *Tissue and electrode capacitance reduce neural activation volumes during deep brain stimulation*. Clinical Neurophysiology, 2005. 116(10): p. 2490-2500.
10. Voon, V., et al., *Deep brain stimulation: Neuropsychological and neuropsychiatric issues*. Movement Disorders, 2006. 21(S14): p. S305-S327.

11. Cheong, W.F., S.A. Prael, and A.J. Welch, *A review of the optical properties of biological tissues*. Quantum Electronics, IEEE Journal of, 1990. 26(12): p. 2166-2185.
12. Arenkiel, B.R., et al., *In Vivo Light-Induced Activation of Neural Circuitry in Transgenic Mice Expressing Channelrhodopsin-2*. Neuron, 2007. 54(2): p. 205-218.
13. Alexander, M.A., et al., *An optical neural interface: in vivo control of rodent motor cortex with integrated fiberoptic and optogenetic technology*. J. Neural Eng., 2007. 4(3): p. S143.
14. Han, X., et al., *Millisecond-Timescale Optical Control of Neural Dynamics in the Nonhuman Primate Brain*. Neuron, 2009. 62(2): p. 191-198.
15. Cao, H., et al., *An Integrated microLED Optrode for Optogenetic Stimulation and Electrical Recording*. IEEE Trans Biomed Eng, 2012.
16. Zhang, F., et al., *Red-shifted optogenetic excitation: a tool for fast neural control derived from *Volvox carteri**. Nat Neurosci, 2008. 11(6): p. 631-633.
17. Gunaydin, L.A., et al., *Ultrafast optogenetic control*. Nat Neurosci, 2010. 13(3): p. 387-392.
18. Lin, J.Y., et al., *Characterization of Engineered Channelrhodopsin Variants with Improved Properties and Kinetics*. Biophys. J., 2009. 96(5): p. 1803-1814.
19. Schmucker, D., et al., *Chromophore-assisted laser inactivation of patched protein switches cell fate in the larval visual system of *Drosophila**. Proc Natl Acad Sci U S A, 1994. 91(7): p. 2664-8.
20. Fenno, L., O. Yizhar, and K. Deisseroth, *The development and application of optogenetics*. Annu Rev Neurosci, 2011. 34: p. 389-412.

21. Peterka, D.S., H. Takahashi, and R. Yuste, *Imaging voltage in neurons*. Neuron, 2011. 69(1): p. 9-21.
22. Stein, W., C. Stadele, and P. Andras, *Optical imaging of neurons in the crab stomatogastric ganglion with voltage-sensitive dyes*. J Vis Exp, 2011(49).
23. Segal, M., *Fast imaging of [Ca]²⁺ reveals presence of voltage-gated calcium channels in dendritic spines of cultured hippocampal neurons*. J Neurophysiol, 1995. 74(1): p. 484-8.
24. Stein, W., C. Stadele, and P. Andras, *Single-sweep voltage-sensitive dye imaging of interacting identified neurons*. J Neurosci Methods, 2011. 194(2): p. 224-34.
25. Hodgkin, A.L. and A.F. Huxley, *A Quantitative Description of Membrane Current and Its Application to Conduction and Excitation in Nerve*. Journal of Physiology-London, 1952. 117(4): p. 500-544.
26. Boyden, E.S., *A history of optogenetics: the development of tools for controlling brain circuits with light*. F1000 Biol Rep, 2011. 3: p. 11.
27. Hodgkin, A.L., *Chance and Design in Electrophysiology - Informal Account of Certain Experiments on Nerve Carried out between 1934 and 1952*. Journal of Physiology-London, 1976. 263(1): p. 1-21.
28. Schroll, C., et al., *Light-induced activation of distinct modulatory neurons triggers appetitive or aversive learning in Drosophila larvae*. Curr Biol, 2006. 16(17): p. 1741-7.
29. Adamantidis, A.R., et al., *Neural substrates of awakening probed with optogenetic control of hypocretin neurons*. Nature, 2007. 450(7168): p. 420-4.

30. Zhang, W., W.P. Ge, and Z.R. Wang, *A toolbox for light control of Drosophila behaviors through Channelrhodopsin 2-mediated photoactivation of targeted neurons*. European Journal of Neuroscience, 2007. 26(9): p. 2405-2416.
31. Lagali, P.S., et al., *Light-activated channels targeted to ON bipolar cells restore visual function in retinal degeneration*. Nat Neurosci, 2008. 11(6): p. 667-75.
32. Alilain, W.J., et al., *Light-induced rescue of breathing after spinal cord injury*. J Neurosci, 2008. 28(46): p. 11862-70.
33. Mahoney, T.R., et al., *Intestinal signaling to GABAergic neurons regulates a rhythmic behavior in Caenorhabditis elegans*. Proc Natl Acad Sci U S A, 2008. 105(42): p. 16350-5.
34. Han, X., et al., *Millisecond-Timescale Optical Control of Neural Dynamics in the Nonhuman Primate Brain*. Neuron, 2009. 62(2): p. 191-198.
35. Goddard, G.V., D.C. McIntyre, and C.K. Leech, *A permanent change in brain function resulting from daily electrical stimulation*. Exp Neurol, 1969. 25(3): p. 295-330.
36. Lozano, A.M., et al., *Deep brain stimulation for Parkinson's disease: disrupting the disruption*. Lancet Neurology, 2002. 1(4): p. 225-231.
37. Han, J.S., *Acupuncture: neuropeptide release produced by electrical stimulation of different frequencies*. Trends in Neurosciences, 2003. 26(1): p. 17-22.
38. Mohanty, S.K., et al., *In-depth activation of channelrhodopsin 2-sensitized excitable cells with high spatial resolution using two-photon excitation with a near-infrared laser microbeam*. Biophysical Journal, 2008. 95(8): p. 3916-3926.
39. Rickgauer, J.P. and D.W. Tank, *Two-photon excitation of channelrhodopsin-2 at saturation*. Proc Nat Acad Sci, 2009. 106(35): p. 15025-15030.

40. Andrasfalvy, B.K., et al., *Two-photon single-cell optogenetic control of neuronal activity by sculpted light*. Proceedings of the National Academy of Sciences of the United States of America, 2010. 107(26): p. 11981-11986.
41. Papagiakoumou, E., et al., *Scanless two-photon excitation of channelrhodopsin-2*. Nature Methods, 2010. 7(10): p. 848-U117.
42. Xu, C. and W.W. Webb, *Measurement of two-photon excitation cross sections of molecular fluorophores with data from 690 to 1050 nm*. Journal of the Optical Society of America B-Optical Physics, 1996. 13(3): p. 481-491.
43. Shivalingaiah, S., L. Gu, and S.K. Mohanty, *Non-linear stimulation of excitable cells with and without optogenetic sensitization*. Proc. SPIE 2011. 7883: p. 788355.
44. Murphy, D.B. and M.W. Davidson, *Fundamentals of light microscopy and electronic imaging*. 2nd ed. 2013, Hoboken, N.J.: Wiley-Blackwell. p.
45. Dragomir, A., J.G. McInerney, and D.N. Nikogosyan, *Femtosecond measurements of two-photon absorption coefficients at $\lambda = 264$ nm in glasses, crystals, and liquids (vol 41, pg 4365, 2002)*. Applied Optics, 2002. 41(27): p. 5655-5655.
46. Weik, M.H., *Fiber optics standard dictionary*. 3rd ed. 1997, New York: Chapman & Hall. xxiii, 1218 p.
47. Flock, S.T., B.C. Wilson, and M.S. Patterson, *Monte Carlo modeling of light propagation in highly scattering tissues--II: Comparison with measurements in phantoms*. IEEE Trans Biomed Eng, 1989. 36(12): p. 1169-73.
48. Wang, L.H., S.L. Jacques, and L.Q. Zheng, *Mcm1 - Monte-Carlo Modeling of Light Transport in Multilayered Tissues*. Computer Methods and Programs in Biomedicine, 1995. 47(2): p. 131-146.

49. Wilson, B.C. and G. Adam, *A Monte Carlo model for the absorption and flux distributions of light in tissue*. Med Phys, 1983. 10(6): p. 824-30.
50. Fukui, Y., Y. Ajichi, and E. Okada, *Monte Carlo prediction of near-infrared light propagation in realistic adult and neonatal head models*. Appl Opt, 2003. 42(16): p. 2881-7.
51. McCormick, D.A. and H.C. Pape, *Properties of a hyperpolarization-activated cation current and its role in rhythmic oscillation in thalamic relay neurones*. J Physiol, 1990. 431: p. 291-318.
52. Rhoht , P.e.a., *Two-photon optogenetic toolbox for fast inhibition, excitation and bistable modulation*. Nat. Method, 2012(2012/11/11/online).
53. Nemet, B.A., V. Nikolenko, and R. Yuste, *Second harmonic imaging of membrane potential of neurons with retinal*. Journal of Biomedical Optics, 2004. 9(5): p. 873-881.
54. Farah, N., Matar, S., Marom, A., Golan, L. & Shoham, S., *Photo-absorber based neural stimulation for an optical retinal prosthesis*. . Res. Vis. Opth. (ARVO) 2010.
55. Berndt, A., et al., *High-efficiency channelrhodopsins for fast neuronal stimulation at low light levels*. Proc Natl Acad Sci U S A, 2011. 108(18): p. 7595-600.
56. Schmitt, C., et al., *Specific expression of channelrhodopsin-2 in single neurons of Caenorhabditis elegans*. PLoS One, 2012. 7(8): p. e43164.
57. Kiselev, A. and S. Subramaniam, *Activation and regeneration of rhodopsin in the insect visual cycle*. Science, 1994. 266(5189): p. 1369-73.
58. Braun, F.J. and P. Hegemann, *Two light-activated conductances in the eye of the green alga Volvox carteri*. Biophysical Journal, 1999. 76(3): p. 1668-1678.

59. Nikolic, K., et al., *Photocycles of channelrhodopsin-2*. Photochem Photobiol, 2009. 85(1): p. 400-11.
60. Hegemann, P., W. Gartner, and R. Uhl, *All-trans retinal constitutes the functional chromophore in Chlamydomonas rhodopsin*. Biophys J, 1991. 60(6): p. 1477-89.
61. Nemet, B.A., V. Nikolenko, and R. Yuste, *Second harmonic imaging of membrane potential of neurons with retinal*. J Biomed Opt, 2004. 9(5): p. 873-81.
62. Wang, L., S.L. Jacques, and L. Zheng, *CONV--convolution for responses to a finite diameter photon beam incident on multi-layered tissues*. Comput Methods Programs Biomed, 1997. 54(3): p. 141-50.
63. Johansson, J.D., *Spectroscopic method for determination of the absorption coefficient in brain tissue*. Journal of Biomedical Optics, 2010. 15(5): p. 057005.
64. Yaroslavsky, A.N., et al., *Optical properties of selected native and coagulated human brain tissues in vitro in the visible and near infrared spectral range*. Phys Med Biol, 2002. 47(12): p. 2059-73.
65. Cheong, W.F., S.A. Prael, and A.J. Welch, *A Review of the Optical-Properties of Biological Tissues*. IEEE Journal of Quantum Electronics, 1990. 26(12): p. 2166-2185.
66. Gradinaru, V., et al., *Targeting and readout strategies for fast optical neural control in vitro and in vivo*. Journal of Neuroscience, 2007. 27(52): p. 14231-14238.
67. Albota, M.A., C. Xu, and W.W. Webb, *Two-Photon Fluorescence Excitation Cross Sections of Biomolecular Probes from 690 to 960 nm*. Appl Opt, 1998. 37(31): p. 7352-6.
68. Bestvater, F., et al., *Two-photon fluorescence absorption and emission spectra of dyes relevant for cell imaging*. J Microsc, 2002. 208(Pt 2): p. 108-15.

69. Masters, B.R., P.T. So, and E. Gratton, *Multiphoton excitation microscopy of in vivo human skin. Functional and morphological optical biopsy based on three-dimensional imaging, lifetime measurements and fluorescence spectroscopy*. Ann N Y Acad Sci, 1998. 838: p. 58-67.
70. Shivalingaiah, S., L. Gu, and S.K. Mohanty, *Non-linear stimulation of excitable cells with and without optogenetic sensitization*. Photonic Therapeutics and Diagnostics VII, 2011. 7883.
71. Yamaguchi, S. and T. Tahara, *Two-photon absorption spectrum of all-trans retinal*. Chemical Physics Letters, 2003. 376(1-2): p. 237-243.
72. Vivas, M.G., et al., *Degenerate two-photon absorption in all-trans retinal: nonlinear spectrum and theoretical calculations*. J Phys Chem A, 2010. 114(10): p. 3466-70.
73. Shapiro, M.G., et al., *Infrared light excites cells by changing their electrical capacitance*. Nature Communications, 2012. 3.
74. Hirase, H., et al., *Multiphoton stimulation of neurons*. J. Neurobiol., 2002. 51(3): p. 237-247.
75. Denton, M.L., et al., *Damage thresholds for exposure to NIR and blue lasers in an in vitro RPE cell system*. Investigative Ophthalmology & Visual Science, 2006. 47(7): p. 3065-3073.
76. Widom, B., P. Bhimalapuram, and K. Koga, *The hydrophobic effect*. Physical Chemistry Chemical Physics, 2003. 5(15): p. 3085-3093.
77. Wells, J., et al., *Optical stimulation of neural tissue in vivo*. Opt Lett, 2005. 30(5): p. 504-6.
78. Teudt, I.U., et al., *Optical stimulation of the facial nerve: a new monitoring technique?* Laryngoscope, 2007. 117(9): p. 1641-7.

79. Izzo, A.D., et al., *Laser stimulation of the auditory nerve*. *Lasers Surg Med*, 2006. 38(8): p. 745-53.
80. Harris, D.M., et al., *Optical nerve stimulation for a vestibular prosthesis*. *Proc. SPIE*, 2009: p. 7180, 71800R.
81. Dalkara, D., et al., *Enhanced gene delivery to the neonatal retina through systemic administration of tyrosine-mutated AAV9*. *Gene Ther*, 2011. 19(2): p. 176-81.
82. Cayce, J.M., et al., *Optical Stimulation of the Central Nervous System in vitro*. *Biomedical Optics*, 2008: p. BTuE5.
83. Barnes, F.S., *Cell-Membrane Temperature Rate Sensitivity Predicted from the Nernst Equation*. *Bioelectromagnetics*, 1984. 5(1): p. 113-115.
84. Pettit, D.L., et al., *Chemical two-photon uncaging: a novel approach to mapping glutamate receptors*. *Neuron*, 1997. 19(3): p. 465-71.
85. Wang, J., M.T. Hasan, and H.S. Seung, *Laser-evoked synaptic transmission in cultured hippocampal neurons expressing channelrhodopsin-2 delivered by adeno-associated virus*. *J Neurosci Methods*, 2009. 183(2): p. 165-75.
86. Wilson, B.C. and S.L. Jacques, *Optical reflectance and transmittance of tissues: principles and applications*. *Quantum Electronics, IEEE Journal of*, 1990. 26(12): p. 2186-2199.
87. Jacques, S.L., *Time resolved propagation of ultrashort laser pulses within turbid tissues*. *Appl. Opt.*, 1989. 28(12): p. 2223-2229.
88. Kienle, A., et al., *Spatially resolved absolute diffuse reflectance measurements for noninvasive determination of the optical scattering and absorption coefficients of biological tissue*. *Appl. Opt.*, 1996. 35(13): p. 2304-2314.
89. Kanneganti, A., et al., *Deep Brain Optogenetic Stimulation Using Bessel Beam*

- hys. J., 2011. 100(3): p. 95a.
90. Mishra, Y.N., N. Ingle, and S.K. Mohanty, *Trapping and two-photon fluorescence excitation of microscopic objects using ultrafast single-fiber optical tweezers*. *Journal of Biomedical Optics*, 2011. 16(10): p. 105003.
 91. Goto, Y., et al., *Functional Abnormalities in Transgenic Mice Expressing a Mutant Rhodopsin Gene*. *Investigative Ophthalmology & Visual Science*, 1995. 36(1): p. 62-71.
 92. Keen, T.J., et al., *Autosomal dominant retinitis pigmentosa: four new mutations in rhodopsin, one of them in the retinal attachment site*. *Genomics*, 1991. 11(1): p. 199-205.
 93. Stosiek, C., et al., *In vivo two-photon calcium imaging of neuronal networks*. *Proceedings of the National Academy of Sciences of the United States of America*, 2003. 100(12): p. 7319-7324.
 94. Wu, J.Y., et al., *Voltage-sensitive dyes for monitoring multineuronal activity in the intact central nervous system*. *Histochemical Journal*, 1998. 30(3): p. 169-187.
 95. Eliezer, D., *Biophysical characterization of intrinsically disordered proteins*. *Current Opinion in Structural Biology*, 2009. 19(1): p. 23-30.

Biographical Information

Kamal Raj Dhakal was born in India but raised in Phaparthum-7, Syangja, Nepal. He received his Bachelor's degree in Physics from Tribhuvan University, Nepal in 2004. He started teaching in his early age for secondary school; Gyan Joti Boarding School, Bhagawati Secondary School and Evergreen Boarding School, Syangaj. He graduated (MS major Physics) from Tribhuvan University in 2007. Kamal was also involved in extra-activities. He was the president of youth club (Suryo Daya Youth Club) in his village. He also elected as treasurer in Student Association of Physics Student (SAPS) in his MS. He was also editor of Magazine "Symmetry" which publishes yearly from the Department of Physics, Tribhuvan University, Nepal. After Competing Master, He started working as Lecturer at Central Department of Environment Science in Tribhuvan University, Kirtipur and St. Xavier's College, Maitighar Kathmandu Nepal from 2007-2010.

In 2010, He came in University of Rhode Island, RI, USA for his PhD. Being interested in Bio- Physics; He transferred to UTA in 2011. He started working in Optogenetics after joining Dr. Mohanty's lab. After MS, he will pursue his PhD in related field.